

Accounts

Molecule-Based Magnets in Heterospin Systems

Noboru Koga* and Satoru Karasawa

Graduate School of Pharmaceutical Sciences, Kyushu University, 3-1-1 Maidashi, Higashi-ku, Fukuoka 812-8582

Received January 20, 2005; E-mail: koga@phar.kyushu-u.ac.jp

Our approaches to the molecule-based magnets by using heterospin systems are reviewed. In our heterospin systems consisting of the organic 2p spins and the metal ion 3d spins, various pyridines carrying the organic spins were used as binding ligands for 3d metal ions. Carbenes generated by photolysis of diazo groups and persistent *N-tert*-butylaminoxyl radicals were employed as the organic spin sources. First, various model complexes were prepared and their magnetic couplings between the organic spin and the metal ion through the pyridine ligand were revealed. Based on the results of magnetic studies on model complexes, ferri- and ferromagnetic complexes having linear chain structures were designed and successfully prepared. When our heterospin systems were used under solution conditions, new fields were opened. Assemblies formed in frozen solution had magnetic behaviors exhibiting slow magnetic relaxations. Especially, when the anisotropic metal ion, high-spin cobalt(II) ion, was used as the metal ion in our heterospin system, the complex formed in frozen solution functioned as a single-molecule magnet (SMM). Such formation of a monometallic SMM was the first example reported.

The molecule-based magnets[1,2] have been studied intensively together with the development of new functional materials. The magnetic properties of molecule-based magnets depend on the dimension of their spin networks. The three-, two-, one-, and zero-dimensional (3D, 2D, 1D, and 0D, respectively) spin networks show individual magnetic behaviors. For example, a bulk ferromagnet requires a 3D spin network and a single-molecule magnet (SMM)[3] which is a current topic of the field of molecule-based magnets requires a 0D one. Low-dimensional spin networks (such as 1D and 2D), especially ones containing anisotropic metal ions also show interesting magnetic behavior, so they have recently become attractive research targets in this field.[4,5] In the construction of molecule-based magnets, therefore, it becomes important to determine how a spin network can be constructed. For the purpose, we proposed to use heterospin systems[6] consisting of organic 2p spins and metal ion 3d spins. Since metal ions can serve as connectors for high-dimensional molecular architecture by bridging the lower dimensional organic ligand molecules used as building blocks, construction of heterospin systems appears to be one of the most promising design strategies for real molecular-based magnets. Previously, the syntheses of ferromagnetic chain and ferri/ferromagnets by using nitronyl nitroxide and *tert*-butylaminoxyl radical units ligated to bis(hexafluoroacetylacetonato)manganese [$Mn(hfac)_2$] were reported by D. Gatteschi[7] and H. Iwamura.[8] In these cases, however, the radical centers also serve as the ligating centers (L = S; see Scheme 1) and it is difficult to control the sign of the exchange coupling between the spins of the metals and the organic radicals. Our alternative strategy is based on the idea that, when transition metals (M) are coordinated with certain π-conjugated (L–S) ligand carrying π-radical centers (S) remote from the ligating centers (L), the sign of the magnetic interaction between the spin centers might be controlled by a through-ligand interaction. The 0D-, 1D-, 2D-, and 3D-spin networks in our heterospin systems are schematically illustrated in Scheme 1.

In our heterospin systems, the selections of π-conjugated ligand (L) and organic spin source (S) are important. We selected pyridines for π-conjugated ligand (L), and aminoxyls and carbenes as organic spin sources (S). Various pyridines and polypyridines were used as building blocks for the supramolecular chemistry[9] and the structures and functions of their metal complexes were investigated extensively. In two organic spin sources, *N-tert*-butylaminoxyl is well known to be a persistent radical,[10] while carbene is a reactive intermediate[11] and is unstable at room temperature. Therefore, aminoxyl and carbene were employed for quantitative and qualitative analysis, respectively, of magnetic behavior. Especially, the usage of carbene has several advantages, as follows: 1) Diarylcarbene has triplet grand state ($S = 2/2$) and is useful to make a high-spin species. 2) Diarylcarbene has a versatile skeletal and electronic structure in which two aryl groups are attached to the carbene center and the p-spin is effectively delocalized on the both-side rings. These facts make possible the basic framework (L···S···L) for high-dimensional spin network by replacing terminal phenyl rings in pure polycarbene with pyridyl rings (see Scheme 2a). 3) The most interesting benefit is the addition of photoresponsiveness to the magnetism. The role of the diazo/carbene combination as a photoresponsive magnetic coupler is summarized in Scheme 2b.

Published on the web August 4, 2005; DOI 10.1246/bcsj.78.1384

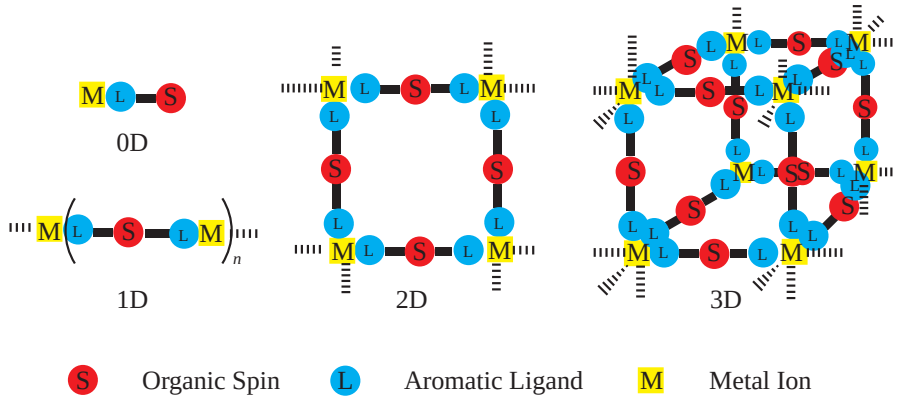

Scheme 1. The 0D-, 1D-, 2D-, and 3D-spin networks in our heterospin systems.

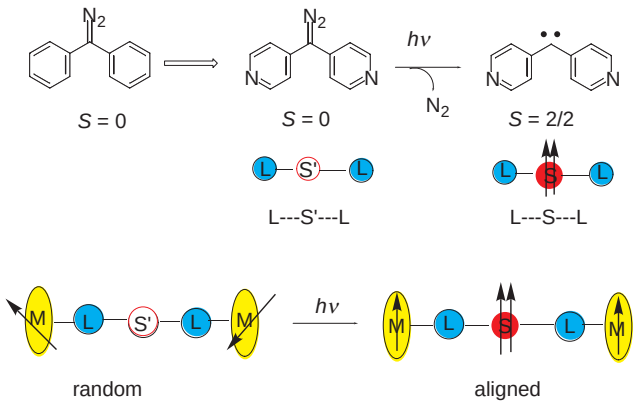

Scheme 2. a) Molecular design for a photoresponsive magnetic coupler (PMC) and b) role of diazo/carbene as PMC.

As shown in Scheme 2a, carbenes act not only as organic spin sources but also as magnetic couplers. Two metal ions have no magnetic interaction before irradiation, while they start to interact through the generated carbene after irradiation. Therefore, we call such a diazo pyridine(s) compound a photoresponsive magnetic coupler (PMC). The characteristic roles of diazo/carbene will be seen in sections **2** and **3**. As mentioned later, however, the use of carbene is a double-edged sword in experimental work. We obtain the function of photoresponsiveness at the expense of the quantitativeness in the experiment; it is very difficult to photolyze a sample completely in most cases, especially in solid state. Therefore, two organic spin sources, aminoxyl and carbene, were used properly for the purpose.

Based on these consideration and on some fundamental studies on the organic high-spin molecule, pyridines carrying aminoxyls and diazo moieties were designed and prepared for our heterospin systems. The typical pyridine derivatives are shown in Chart 1.

These pyridine-organic spin derivatives (L···S and L···S···L) make possible the uses of various metal ions (MXn) and metal complexes (ML′) for our purposes. This is a big advantage of our heterospin system. Monopyridine derivatives were used for the investigation of magnetic coupling between organic spin and metal ion, and for the formation of heterospin complex with high-spin ground states. In pyridine-diazo derivatives, it is confirmed that the carbene centers generated by photolysis of diazo moieties interact ferromagnetically to form the high-spin ground states. Namely, mono-, di-, and tridiazo derivatives produce triplet ($S = 2/2$), quintet ($S = 4/2$), and septet ($S = 6/2$) ground states, respectively. Therefore, it is easy to increase the total spin multiplicity of the complex by changing organic spin units systematically (1 in Scheme 3). On the other hand, di- and tripyridine derivatives were used for the construction of high dimensional spin networks (2 and 3 in Scheme 3). Our approaches to the construction of molecule-based magnet sare shown schematically in Scheme 3.

In the beginning of our heterospin work, we employed crystalline samples for photolysis. We often met problems associated with optical transparency of the diazo samples. To overcome these difficulties, we were forced to use the frozen solution systems for the SQUID measurements. In frozen solution, two new factors have to be taken into account. One is dissociation of the metal complexes. Generally, 2,2′-bipyridine ligands having high association constants with various metal ions will be favorable in this respect. Secondly, a small amount of paramagnetic species and a large amount of diamagnetic solvent molecules are present in the sample and they magnetically compete with each other. Especially, it is difficult in a sample for paramagnetic species with a small S value. A problem for a magnetic experiment in frozen solution lies in how accurately a diamagnetic contribution of the solvent in a sample is estimated. In our diazo/carbene system, however, the problem can be resolved by using the difference of magnetizations (M) before and after irradiation without touching the

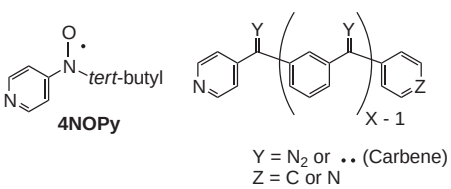

D1Py; X = 1, Y = N_2, Z = C
C1Py; X = 1, Y = ••, Z = C
D2Py; X = 2, Y = N_2, Z = C
C2Py; X = 2, Y = ••, Z = C
D3IPy; X = 3, Y = N_2, Z = C
C3IPy; X = 3, Y = ••, Z = C

D1Py2; X = 1, Y = N_2, Z = N
C1Py2; X = 1, Y = ••, Z = N
D2Py2; X = 2, Y = N_2, Z = N
C2Py2; X = 2, Y = ••, Z = N
D3IPy2; X = 3, Y = N_2, Z = N
C3IPy2; X = 3, Y = ••, Z = N

Chart 1. **4NOPy**, **DXPy**, and **DXPy2** derivatives.

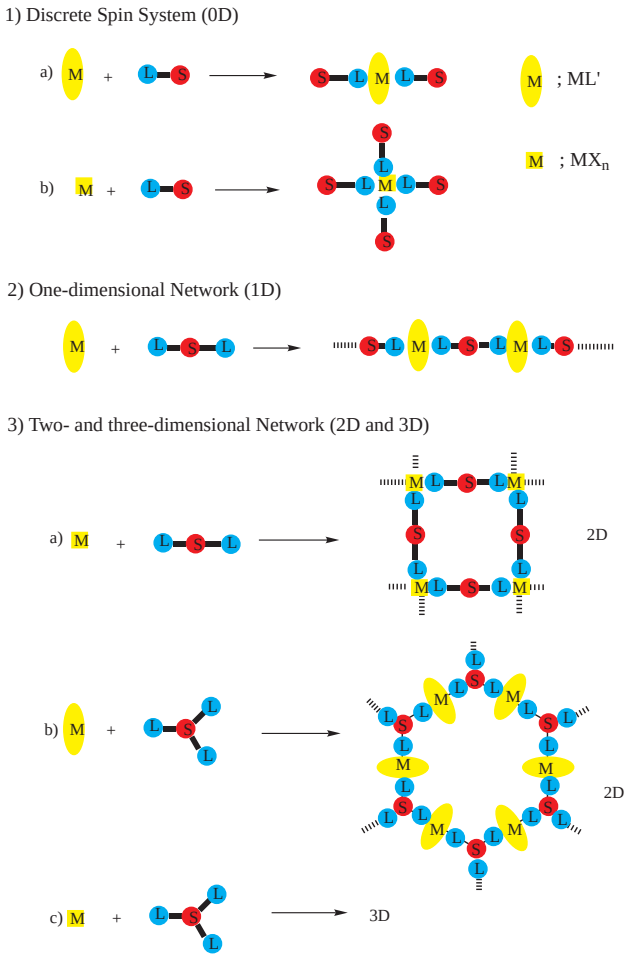

Scheme 3. Strategies for the construction of 0D, 1D, 2D, and 3D spin networks in our heterospin system.

sample inbetween. An additional advantage of a frozen solution condition is that the intermolecular antiferromagnetic interaction, which is often observed at a low temperature region (<10 K) in a crystal sample, can be neglected.

The frozen solution condition which will produce a zero dimensional (0D) network is unfavorable for the construction of a bulk ferromagnet. During 1993, an Mn12 cluster[12] with $S = 10$ was reported as single-molecule magnets (SMMs) exhibiting a slow magnetic relaxation. Since then, various metal clusters containing V,[13] Mn,[14] Fe,[15] Co,[16] and Ni[17] ions for 3d metals and Tb and Dy for 4f metals[18] have been reported as SMMs. This SMM shows a hysteresis loop of magnetization at extremely low temperature, similar to the one for a bulk ferromagnet. Our heterospin system in frozen solution was found to be suitable for the construction of SMM.

In the first part (section **1**) of this paper, the studies of magnetic interactions between organic spin and metal spin in the 1:2 complexes (S···L–M–L···S) of paramagnetic 3d metal ions with pyridine ligand having a *N-tert*-butylaminoxyl radical or a diazo group (**4-** and **3NOPy**, and **D1Py**, respectively) are reported. It is of particular interest to see if the regiospecificity found in organic *p*-diradicals like quinodimethanes (***p*** vs ***m*** in Scheme 4) is also applicable to the interaction between free radical centers (S) and coordinated magnetic metal ions (M)

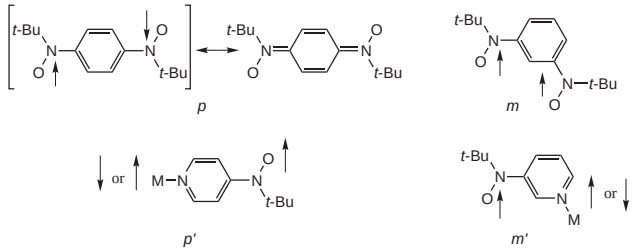

Scheme 4. Regiospecificity in organic spin and heterospin system.

that are separated by π-conjugated ligands as in S···L···M (***p'*** vs ***m'*** in Scheme 4). Furthermore, the sign and magnitude of the exchange interaction between the two components in metal-radical heterospin systems are expected to depend not only on the periodicity of the ligand p orbitals, but also strongly on the magnetic orbitals occupied by the unpaired d electrons of the metal ion.

On the basis of the above knowledge, a 1D spin network was designed. A strategy of assembling the carbene centers into a rigid polymeric metal complex, $(\cdots L\cdots S\cdots L\text{–}M\cdots)_n$, (see 1D in Scheme 1) by using coordinatively doubly unsaturated paramagnetic metal ions with bridging ligands was taken. For the purpose, diazodi(4-pyridyl)methane, **D1Py2**, having two pyridine groups and M(hfac)$_2$; M = Cu and Mn were used. The formations of ferro- and ferrimagnetic super-high-spin chains after photolysis are described in section **2**. In order to increase the dimension of the spin-networks from 1D to 2D and/or 3D structures, two approaches can be considered; one is the use of coordinatively highly-unsaturated metal ion without hfac ligand and the other is the design of highly branched base ligands. Each idea is schematically shown in parts a), b), and c) of 3) of Scheme 3.

We have found new assemblies exhibiting interesting magnetic behavior in frozen solution. The frozen solution condition employed for effective photolysis of diazo moieties is a condition similar to the one used for the formation of high-spin polycarbene in the early stages of our work. As described in section **4**, some assemblies formed in the combination of M(hfac)$_2$ and branched PMC exhibit spin-glass-like magnetic behaviors after irradiation under frozen solutions. These works led a new approach to the single-molecule magnets (SMMs) by employing an anisotropic metal ion. The slow relaxation for the reorientation of spins in SMM can be understood by the double-well energy potential diagram, in which the positive and negative M_s quantum levels are separated by an activation barrier (Δ/k_B) corresponding to $|DS^2|$; D (<0) is the zero-field splitting parameter and S is the spin quantum number (Fig. 1).

Therefore, the construction of SMM has two requirements: 1) the complex has a large $|DS^2|$ value in the ground state and 2) since the origin of the magnetic property of SMM is essentially due to the one molecule, the complex has to be magnetically isolated. To answer these two requirements for SMM, our heterospin systems containing anisotropic metal ions and organic spins with high-spin ground state in frozen solution were applied. As shown in the strategy for 0D spin network (Scheme 3), two approaches were employed. In section **5**, the monometallic SMMs having relatively large Δ/k_B values (30–90 K) for flipping the spins will be discussed.

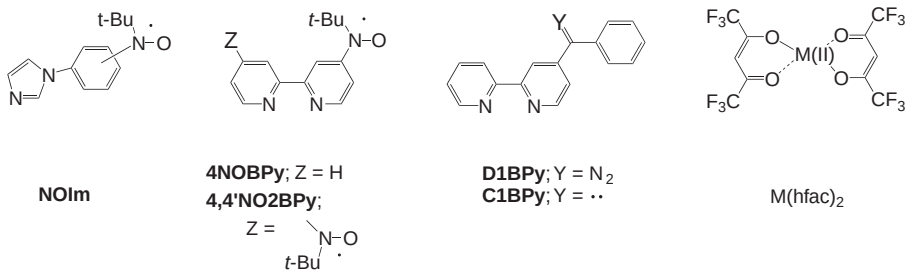

Chart 2.

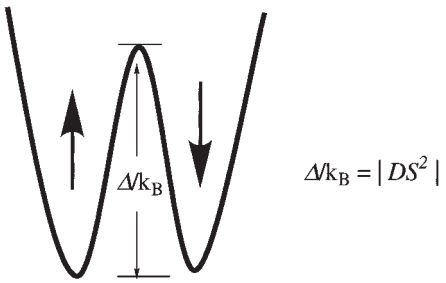

Fig. 1. Energy potential diagram for SMM.

1. 1:2 Model Complexes, S–L···M···L–S

1.1 Molecular Structures of 1:2 Model Complexes. For investigation of the magnetic coupling between the radical center and the metal ion through aromatic ligand, we selected aminoxyl pyridine derivatives, **4NOPy** and **3NOPy** as the appropriate ligands. In this work, the combinations of **NOPy** and **D1Py** (see Chart 1), and bis(hexafluoroacetylacetonate)-metal(II), M(hfac)$_2$; M = Mn, Co, Ni, and Cu, were mainly employed. To investigate the effect of π-conjugated ligand, furthermore, we also selected imidazole and 2,2′-bipyridine carrying aminoxyl, **NOIm** and **4NOBPy** (Chart 1).

By mixing two solutions of M(hfac)$_2$ (M = Mn, Co, Ni, Cu, and Zn) and **NOPy** in a 1:2 ratio, we obtained the complexes of [M(hfac)$_2$·(**NOPy**)$_2$] as single crystals.[19–21] The molecular structures and the crystal packing of all complexes were revealed by X-ray crystal structure analysis. The molecular structures of the copper–pyridine complexes, [Cu(hfac)$_2$·(**4NOPy**)$_2$] and [Cu(hfac)$_2$·(**D1Py**)$_2$] are shown in Fig. 2 together with those for copper–2,2′-bipyridine complexes, [Cu(hfac)$_2$·(**4NOBPy**)] and [Cu(hfac)$_2$·(**D1BPy**)].

As demonstrated in Fig. 2, the molecular structures of all complexes of M(hfac)$_2$ are similar; coordination geometries are elongated and/or distorted octahedra and two pyridyl nitrogen atoms are coordinated to the metal ion in the *trans* configuration. Bond lengths between metal and pyridyl nitrogen and dihedral angles between pyridyl ring and aminoxyl plane for all complexes are listed in Table 1. Those values might affect the magnetic coupling between metal ion and aminoxyl. In crystal packings of the single crystal, all complexes have short contacts (within 5 Å) between neighboring molecules. Especially, in **3NOPy** and **NOBPy** complexes, radical centers are intermolecularly close enough to each other to form the chain and the dimer structures.

1.2 Exchange Coupling between Metal Ion and Radical Center. In order to understand the magnetic coupling quan-

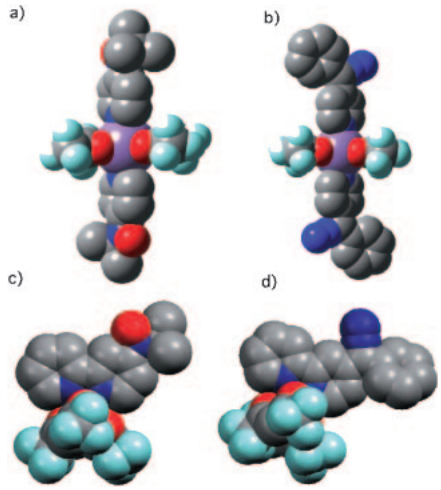

Fig. 2. Molecular structures of a) [Cu(hfac)$_2$·(**4NOPy**)$_2$], b) [Cu(hfac)$_2$·(**D1Py**)$_2$], c) [Cu(hfac)$_2$·(**4NOBPy**)], and d) [Cu(hfac)$_2$·(**D1BPy**)].

titatively, the magnetic susceptibility data of [M(hfac)$_2$·(**4NOPy**)$_2$] were obtained in the temperature range 2–300 K at a constant field of 100 mT. Temperature dependences of $\chi_{mol}T$ values for [Cu(hfac)$_2$·(**4NOPy**)$_2$ and (**3NOPy**)$_2$] and [Mn(hfac)$_2$·(**4NOPy**)$_2$] are shown in Figs. 3a and 3b, respectively.

The $\chi_{mol}T$ values for [Mn(hfac)$_2$·(**4NOPy**)$_2$] and [Cu(hfac)$_2$·(**4NOPy**)$_2$] at 290 K and 300 K are 5.04 and 1.29 emu·K·mol^{-1}, respectively, which are close to the theoretical ones (5.12 and 1.13) calculated in terms of the spin-only equation with Mn(II) and Cu(II) with $S = 5/2$ and $1/2$, respectively, and two aminoxyls with $S = 1/2$. As the temperature was decreased from 300 to 2 K, the $\chi_{mol}T$ values for Mn and Cu complexes gradually decreased and increased, respectively. These temperature profiles of $\chi_{mol}T$ observed in the $\chi_{mol}T$ vs T plots for both Mn and Cu complexes are typical ones for anti- and ferromagnetic interaction, respectively. The steep decreases below 10 K are due to the intermolecular antiferromagnetic interaction. The obtained $\chi_{mol}T$ vs T plots were analyzed by means of theoretical equations for the three-spin model consisting of one metal ion and two aminoxyls. Best-fit parameters are $J/k_B = -12.4$ and 60.4 K, $g = 2.059$ and 2.048, and $\theta = -2.58$ and -3.58 K for Mn and Cu complexes, respectively. On the other hand, the $\chi_{mol}T$ values of isomeric [Cu(hfac)$_2$·(**3NOPy**)$_2$] were nearly constant at 0.5 emu·K·mol^{-1} in the temperature range 5–300 K. This thermal profile of the $\chi_{mol}T$ values was strongly affected by the short

Table 1. Exchange Coupling Constants (J_{R-M}), Bond Lengths, and Dihedral Angles in Various Metal Complexes

Complexes	Jk_B^{-1}/K	M···N_{py} distance/Å	Dihedral angle[a)]/°	Ref.
[Mn(hfac)$_2$·(**4NOPy**)$_2$]	−12.4	2.268	1.7	19
[Mn(hfac)$_2$·(**3NOPy**)$_2$]	?			
[Co(hfac)$_2$·(**4NOPy**)$_2$]	+20.6	2.169	2.9	20
[Ni(hfac)$_2$·(**4NOPy**)$_2$]	+47	2.114	6.2	20
[Cu(hfac)$_2$·(**4NOPy**)$_2$]	+60	2.045	10	21
[Cu(hfac)$_2$·(**3NOPy**)$_2$]	—	2.070	39	
[Mn(hfac)$_2$·(**4NOIm**)]	+4.3[b)]		27	22
[Mn(hfac)$_2$·(**3NOIm**)]	−2.7[b)]		24	
[Cu(hfac)$_2$·(**4NOIm**)$_2$]	+2.3		27	21
[Cu(hfac)$_2$·(**3NOIm**)$_2$]	−0.9		24	
[Mn(hfac)$_2$·**4NOBPy**]	−20.2	2.215, 2.229	18.07	23
[Cu(hfac)$_2$·**4NOBPy**]	+68.7	1.982, 2.012	22.76	23
[Mn(hfac)$_2$·**4,4′NO$_2$BPy**]	−19.1	2.240	16.83	24
[Cu(hfac)$_2$·**4,4′NO$_2$BPy**]	+73	1.992, 1.998	33.09, 15.35	24
[Mn(hfac)$_2$·(**C1Py**)$_2$]	−18	2.280	?	25
[Cu(hfac)$_2$·(**C1Py**)$_2$]	+	1.993		26
[Cu(hfac)$_2$·(**C1BPy**)]	+[c)]	1.999, 1.983		27
[CrTPP(**4NOPy**)Cl][d)]	−77			19
[CrTPP(**3NOPy**)Cl]	+12.3			28

a) Between pyridine ring and aminoxyl plane. b) Between Mn–Mn. c) In frozen solution. d) TPP; tetraphenylporphyrin.

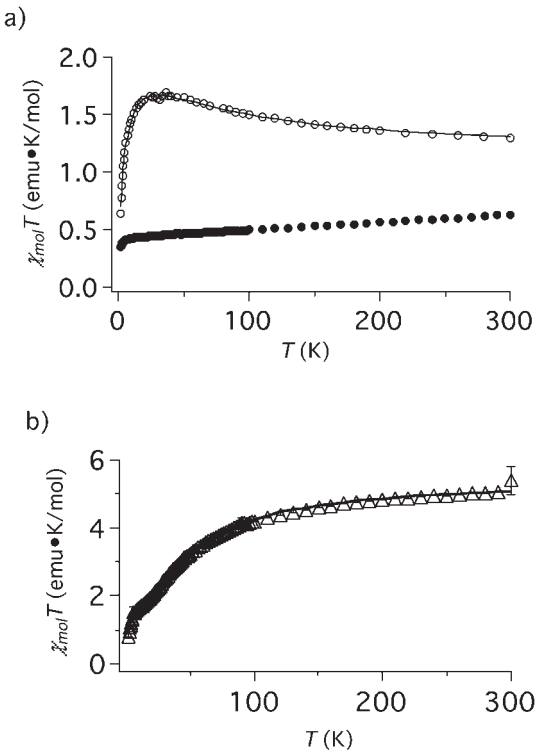

Fig. 3. $\chi_{mol}T$ vs T plots of a) [Cu(hfac)$_2$·(**4NOPy**)$_2$] (○) and [Cu(hfac)$_2$·(**3NOPy**)$_2$] (●) and b) [Mn(hfac)$_2$·(**4NOPy**)$_2$]. The solid lines show theoretical values.

contacts (<3 Å) between aminoxyl centers observed in crystal structure of [Cu(hfac)$_2$·(**3NOPy**)$_2$].

The magnetic susceptibilities of other complexes were also measured under the conditions similar to the ones for [Mn- and Cu(hfac)$_2$·(**4NOPy**)$_2$].[19,21] In the Mn- and Cu(hfac)$_2$-**NOIm** systems, the similar magnetic behaviors were observed. The manganese complexes, [Mn(hfac)$_2$·(**4NOIm** and **3NOIm**)],[22] which have the 1:1 head-to-tail dimer structures, showed ferro- and antiferromagnetic behaviors, respectively (Fig. 4). In the 1:2 complexes of [Cu(hfac)$_2$·(**4NOIm** and **3NOIm**)$_2$],[21] weak ferro- and presumably antiferromagnetic interactions between the copper ion and the aminoxyl radical, respectively were observed. The attenuated interactions are ascribed to the weakened through-bond exchange coupling due to the presence of too many intervening π bonds.

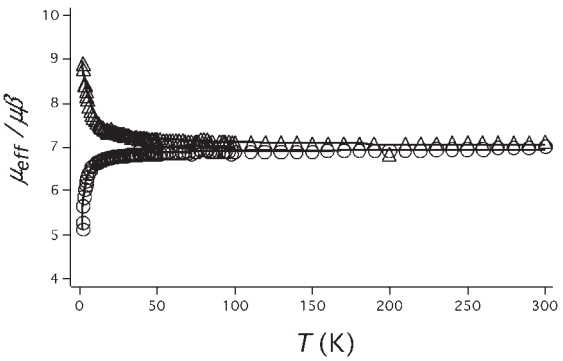

Fig. 4. μ_{eff} vs T plot of [Mn(hfac)$_2$·(**4NOIm**)] (△) and [Mn(hfac)$_2$·(**3NOIm**)] (○).

The magnetic properties of M(hfac)$_2$-**4NOBPy** and M(hfac)$_2$-**4,4′NO$_2$BPy** systems were also investigated under similar conditions. In the $\chi_{mol}T$ vs T plots for [Cu(hfac)$_2$·(**4NOBPy**)] and [Mn(hfac)$_2$·(**4NOBPy**)] (Fig. 5), similar magnetic behaviors were observed; ferro- and antiferromagnetic interactions between the metal ion and the aminoxyl radical in the copper and manganese complexes, respectively. Exper-

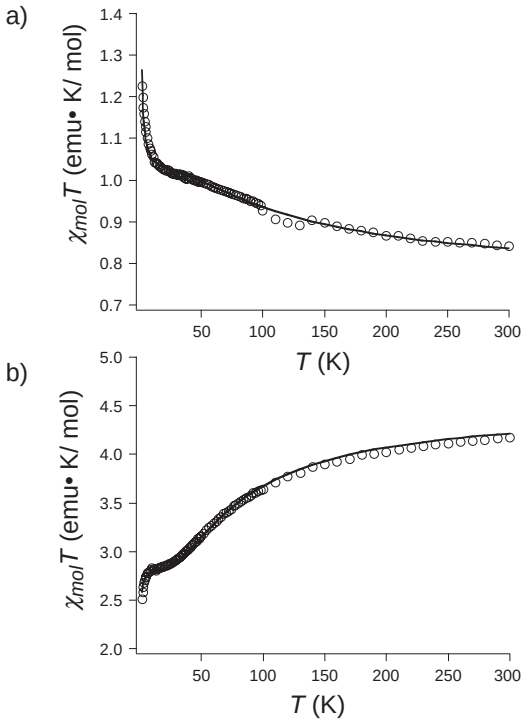

Fig. 5. $\chi_{mol}T$ vs T plots of a) [Cu(hfac)$_2$•(**4NOBPy**)] and b) [Mn(hfac)$_2$•(**4NOBPy**)].

imental data for [Cu(hfac)$_2$•(**4NOBPy**)] and [Mn(hfac)$_2$•(**4NOBPy**)] were analyzed by the two-spin models to give $J/k_B = 68.7$ and -20.2 K, respectively.[23] Data for [Cu(hfac)$_2$•(**4,4′NO$_2$BPy**)] and [Mn(hfac)$_2$•(**4,4′NO$_2$BPy**)] were analyzed by isosceles triangle models to afford $J/k_B = -19.1$ and 73 K, respectively.[24] As listed in Table 1, the magnitudes of J/k_B values for M(hfac)$_2$-2,2′-bipyridine systems are larger than the ones for the corresponding monopyridine systems.

When the carbene is used as organic spin source, photolysis of diazo moieties has to be conducted at a low temperature (<10 K) inside a SQUID apparatus. For the purpose, a handmade sample holder which would allow the irradiation of the sample by using an outside Argon laser ($\lambda = 514$ nm) through an optical fiber was used. Our irradiation system is schematically shown in Fig. 6.[25–27]

The magnetic properties before and after irradiation of the crystalline samples of [Mn- and Cu(hfac)$_2$•(**D1Py**)$_2$] were investigated. When irradiation started, the values of the magnetic susceptibilities for [Mn- and Cu(hfac)$_2$•(**D1Py**)$_2$] at 5 K in a constant field of 5 kOe gradually decreased and increased, respectively.[25,26] The obtained temperature dependence of $\chi_{mol}T$ values below 100 K after irradiation for 5 h suggests that anti- and ferromagnetic interactions take place in the manganese and copper complexes, respectively. As an example, the $\chi_{mol}T$ vs T plots of before and after irradiation of [Mn(hfac)$_2$•(**D1Py**)$_2$] are shown in Fig. 7. The theoretical equation for three-spin model ($S_1 \cdots S_{Mn} \cdots S_1$) fitted the experimental data after irradiation for 18 h to afford the $J/k_B = -18$ K.

The magnetic properties before and after irradiation of [Cu(hfac)$_2$•(**D1BPy**)] in frozen MTHF solution were investi-

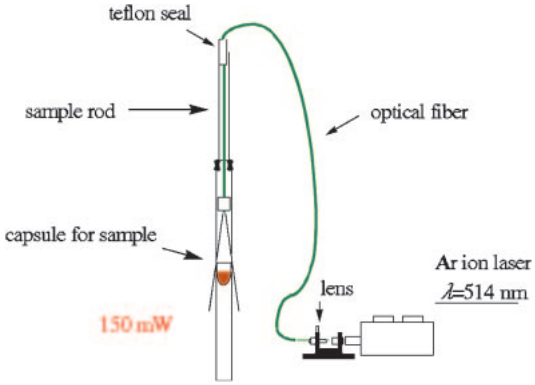

Fig. 6. Irradiation system for SQUID measurements.

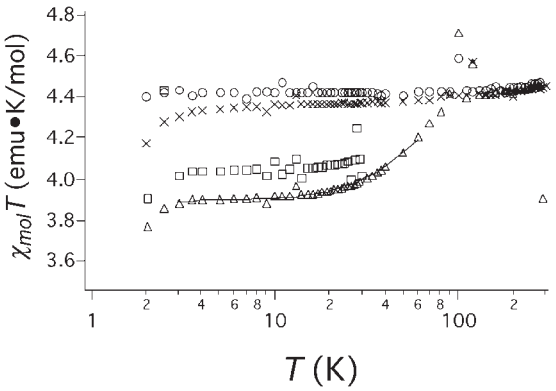

Fig. 7. $\chi_{mol}T$ vs T plot of before (○), after irradiation of [Mn(hfac)$_2$•(**D1Py**)$_2$] for 2 (□) and 18 h (△), and then after annealing (×) at 300 K. The solid line shows the theoretical result.

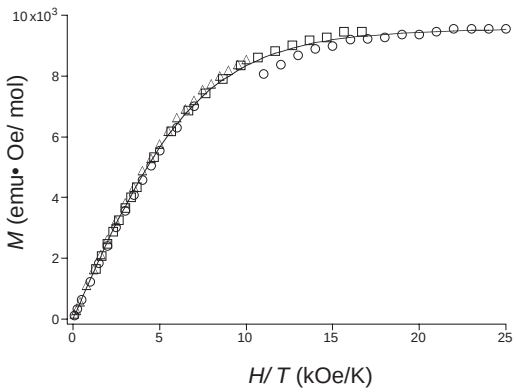

Fig. 8. M vs H/T plot for the MTHF solution sample of [Cu(hfac)$_2$•**C1BPy**] at 2.0 (○), 3.0 (□), and 5.0 K (△). The solid line shows the theoretical result caluculated with $S = 1.53$ and $F = 0.87$.

gated by EPR spectrometry and SQUID magneto/susceptometry. The field dependence of Magnetization (M) after irradiation for 90 min of a frozen-solution sample of [Cu(hfac)$_2$•(**D1BPy**)][27] is shown in Fig. 8. The theoretical equation was fitted to the experimental data to give $S = 1.53$ ($F = 0.87$), indicating that generating carbene interacts with copper ion ferromagnetically to form a high-spin complex with a quartet ground state.

The obtained exchange coupling parameters (J_{R-C}) for $[M(hfac)_2 \cdot (\mathbf{4NOPy})_2]$[19–21] and related complexes[22–28] are summarized in Table 1 together with their bond lengths ($M \cdots N_{py}$) and the dihedral angles between pyridine ring and aminoxyl plane as revealed by X-ray analysis.

(A) The Comparison Between the Copper and Manganese Complexes. The magnetic interactions between copper(II) and **4NOPy** are unique in that they are ferromagnetic and rather large in magnitude: $J/k_B = 60.4$ K. The couplings of the copper ions attached directly to the aminoxyl radicals via their oxygen atoms are well documented and the materials are typically antiferromagnetic due to the overlap of the singly occupied orbitals of the metal ion and the free radical. Only when the oxygen atom of an aminoxyl radical is axially bound to a tetragonal copper(II) ion does a weak ferromagnetic coupling (~20 K) develop. The relative geometry between the magnetic orbital of the copper(II) ion and the π orbital of the pyridine ring, as revealed by X-ray molecular structure analyses, is illustrated in Fig. 9a.

The magnetic orbital $d_{x^2-y^2}$, orthogonal to the elongated axis of octahedral Cu(II), is directed to the two nitrogen atoms of the pyridine ligands and the oxygen atoms of the two hfac ligands in the 1:2 complexes (Fig. 9a). As seen clearly in Fig. 9a, the magnetic orbital $d_{x^2-y^2}$ of Cu(II) and the p-orbital at the nitrogen atom of the pyridine unit to which the 2p spin is polarized via the p-electrons on the pyridine ring from the aminoxyl radical center should be orthogonal. This orthogonality will be responsible for the ferromagnetic interaction. For the construction of super-high spin molecules in heterospin systems, these considerations lead to an interesting and useful conclusion that a copper(II) ion in normal 5- and 6-coordination induces a parallel spin on the ligating atom of a conjugated π-ligand such as pyridine. There is one important precedent for such ferromagnetic coupling in the copper(II) complex with 2-(2-pyridyl)-4,4,5,5-tetramethyl-4,5-dihydro-1*H*-imidazolyl-1-oxyl, in which both the imino and pyridyl nitrogens are attached to the copper ion as a bidentate ligand and the ferromagnetic coupling is as strong as >215 K.[29] In this case, the delocalization of the spin by the contribution of an aminyl–nitrone resonance hybrid and the proximity of the imino nitrogen atom with respect to the aminoxyl radical center which facilitate the spin polarization at the imino nitrogen appear to be responsible for the stronger ferromagnetic coupling.

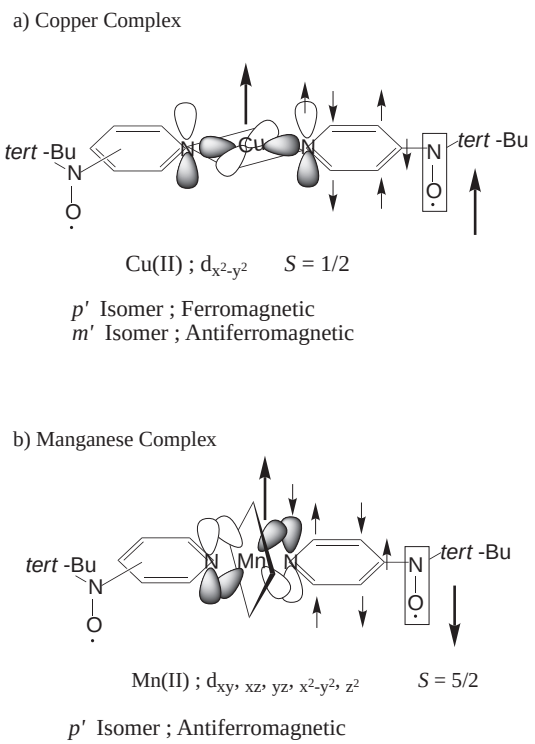

Fig. 9. Interactions between aminoxyl and a) copper(II) ion and b) manganese(II) ion.

When the molecular structure (Fig. 2a) of $[Cu(hfac)_2(\mathbf{4NOPy})_2]$ is compared with those of the corresponding manganese complexes, e.g. $[Mn(hfac)_2(\mathbf{4NOPy})_2]$, we note that both the complexes have similar molecular structures in which nitrogen atoms of two **4NOPy**s are coordinated to the metal ion in the *trans* configuration. However, when the J/k_B values of both the complexes are compared, the signs are opposite: positive for the former and negative for the latter with $J/k_B = 60.4$ and -12.4 K for $[Cu(hfac)_2(\mathbf{4NOPy})_2]$ and $[Mn(hfac)_2(\mathbf{4NOPy})_2]$, respectively. Furthermore, we note that the magnitude for the copper(II) ion is about five times larger than the one for the manganese complex. The dihedral angles between the *N-tert*-butylaminoxyl plane and the pyridine ring are 10° and 1.7° for $[Cu(hfac)_2(\mathbf{4NOPy})_2]$ and $[Mn(hfac)_2(\mathbf{4NOPy})_2]$, respectively, and thus do not explain the difference. Therefore, the difference in the J/k_B values between the copper and the manganese complexes is considered to be derived from the magnetic d orbitals occupied by the unpaired electrons in the metal ions, $d_{x^2-y^2}$ for copper(II) ions and d_{xy}, d_{yz}, d_{xz}, $d_{x^2-y^2}$, and d_{z^2} for manganese(II) ions. The coordination geometry of the $[Mn(hfac)_2(\mathbf{4NOPy})_2]$ complex is a slightly elongated octahedron in which the axial ligands are the nitrogen atoms of the pyridine groups. Therefore, the magnetic orbitals of manganese(II) ion can overlap with the p orbital at the nitrogen on the pyridine ring (Fig. 9b) to produce an antiferromagnetic interaction with the spin on nitrogen transmitted in the same way as in the case of the copper complex.

(B) Regiospecificity in Exchange Interaction with Respect to the Aminoxyl Radical Site on the Pyridine Ring. Now that the magnetic interaction between the organic 2p spins of the aminoxyl or carbene centers on the one hand and 3d spins of metal ions on the other in $[M(hfac)_2(\mathbf{4NOPy}$ or $\mathbf{C1Py})_2]$ complexes has been explained by spin polarization of the p-electrons on the pyridine ring as shown in Fig. 9, such interactions are expected to depend on the site of the aminoxyl or carbene centers on the pyridine ring. Whereas the signs of intramolecular exchange parameter for both Cu- and $Mn(hfac)_2$ complexes ligated with **4NOPy** were determined to be positive and negative, respectively, conclusive results were not obtained for isomeric **3NOPy** complexes because of interference from the strong intermolecular antiferromagnetic interaction. In the **NOIm**–$M(hfac)_2$ systems, similar regiospecificity in the magnetic interactions between the metal ion and the aminoxyl were observed; weak ferro- and presumably antiferromagnetic interactions occur between the copper ion and the aminoxyl radical in $[Cu(hfac)_2(\mathbf{4NOIm}$ and $\mathbf{3NOIm})_2]$, respectively. The expected regiospecificity in the

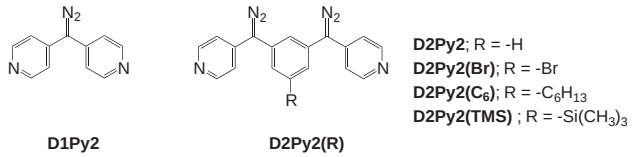

Chart 3.

exchange coupling is clearly found in a reported pair of *meso*-tetraphenylporphyrinatochromium(III) complexes with the isomeric pyridylaminoxyls, Cr(III)TPP(**3**-and **4NOPy**)Cl, although their molecular structure could not yet be determined by X-ray analysis. The chromium(III) ion in the porphyrin complexes has three unpaired electrons on the d_{xy}, d_{xz}, and d_{yz} orbitals each of which is a p magnetic orbital and two (d_{xz} and d_{yz}) of which will be able to overlap with the p orbital of the apical pyridine ring. Therefore, its magnetic coupling can be considered to be similar to that of the manganese(II) ion. The isomeric complexes Cr(TPP)(**3**-and **4NOPy**)Cl show a striking contrast in their intramolecular magnetic interactions; the d^3 electrons of chromium(III)porphyrins and the unpaired 2p electrons on the ligating **3**- and **4NOPy** have been found by EPR and SQUID measurements to interact ferro- and antiferromagnetically to give quintet ($S = 3/2 + 1/2$) and triplet ($S = 3/2 - 1/2$) ground states, respectively.

Thus their magnetic properties revealed that the sign of the exchange interactions between the radical center and the metal ion is controlled by the regiochemistry of the radical center on the pyridine or *N*-phenylimidazole rings, which in turn is explained in terms of the spin polarization mechanism of the p-electrons (Fig. 9).

2. One-Dimensional Spin Network in Heterospin System[26,30,31]

For the construction of spin-network having a chain structure, **D1Py2** and **D2Py2** having two pyridine groups at terminal positions were designed as PMCs and prepared (Chart 3).

2.1 Crystal Structure of 1:1 Complexes of M(hfac)$_2$ and PMCs. The 1:1 manganese(II) and copper(II) complexes, [Mn- and Cu(hfac)$_2$·**D1Py2**] and [Mn- and Cu(hfac)$_2$·**D2Py2(R)**], were prepared in a manner similar to the procedure for 1:2 complexes.[26,30] In both metal complexes of [Mn- and Cu(hfac)$_2$·**D1Py2**], two kinds of crystals, complexes **a** and **b**, were obtained by using different solvents for the recrystallization. Two pyridine groups in [Mn(hfac)$_2$·**D1Py2**][30] of complexes **a** and **b** coordinate with different manganese ions in *trans* and *cis* configuration to form zig-zag and spiral structures, respectively. In the corresponding copper complexes, only complex **a** was analyzed; its crystal structure was close to the one for complex **a** for manganese. The single crystals of [Cu(hfac)$_2$·**D2Py2(Br)**][20] and [Mn(hfac)$_2$·**D2Py2(TMS)**][31] were also obtained and their crystal structures revealed by X-ray analysis were 1D chain structures in which pyridine groups coordinated to the metal ions in *trans* and *cis* configuration, respectively.

The crystal structures of the complexes **a** and **b** in [Mn(hfac)$_2$·**D1Py2**] and [Cu(hfac)$_2$·**D2Py2(Br)**] are shown in Fig. 10.

2.2 Magnetic Measurements of Linear Chain Complexes. The magnetic properties before and after irradiation of the

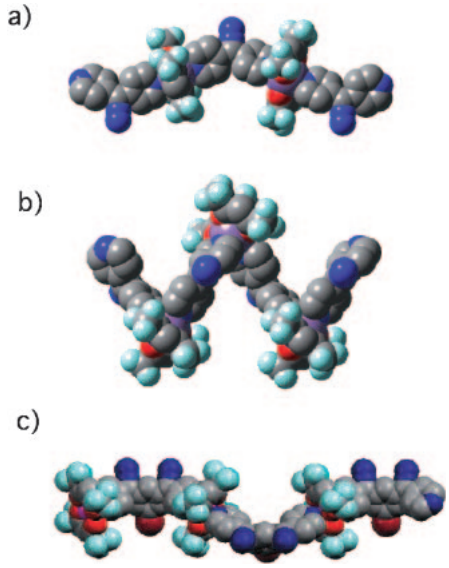

Fig. 10. Crystal structures of a) complex **a** and b) complex **b** in [Mn(hfac)$_2$·**D1Py2**], and c) [Cu(hfac)$_2$·**D2Py2(Br)**].

microcrystalline samples (~0.6 mg) of [Mn- and Cu-(hfac)$_2$·**D1Py2**] and [Mn- and Cu(hfac)$_2$·**D2Py2(TMS)**], were investigated by SQUID magneto/susceptometry under the conditions similar to the ones for the experiments of model complexes. The temperature dependence of $\chi_{mol}T$ values before and after irradiation of [Cu(hfac)$_2$·**D1Py2**] is shown in Fig. 11a. Before irradiation, the $\chi_{mol}T$ values of [Cu-(hfac)$_2$·**D1Py2**] were nearly constant at 0.42 emu·K·mol^{-1} over the temperature range. These values are consistent with $\chi_{mol}T = 0.375$ emu·K·mol^{-1} calculated for a dilute paramagnetic copper(II) of $S = 1/2$, indicating that the d electron spins of copper(II) ions are magnetically isolated. When the complexes were irradiated with an Ar laser ($\lambda = 514$ nm), a drastic difference of the thermal behaviors of $\chi_{mol}T$ values below 230 K was observed in the copper complex. On cooling from 240 K, $\chi_{mol}T$ values of copper complex **a** and **b** continuously increase from 230 K and reached a maximum value of 7.43 and 18.2 emu·K·mol^{-1} at 14 and 3.0 K, respectively, and started to decrease somewhat towards 2 K. The data for complex **a** were analyzed theoretically by the method based on a model of the $S = 1/2$ and $S = 2/2$ Heisenberg ferromagnetic chain to give $J/k_B = +66.8$ K and $g = 2$ for complex **b** of [Cu(hfac)$_2$·**D1Py2**]. The observed sign of exchange coupling between the carbenes and the metal ion is consistent with that prescribed by model complexes. After annealing above 230 K, the thermal behavior in the complex became similar again; the $\chi_{mol}T$ values traced the horizontal line before irradiation. Similarly, the formation of ferrimagnetic chain due to the antiferromagnetic interaction for [Mn(hfac)$_2$·**D1Py2**] was observed after photolysis (Fig. 11b). The theoretical equation fitted the experimental data for complex **a** to gave $J/k_B = -34.8$ K which is close to the one (−17.8 K) for corresponding 1:2 complex. In 1:1 complexes, [Mn- and Cu(hfac)$_2$·**D2Py2-(TMS)**], magnetic behaviors of ferri- and ferromagnetic chains, respectively, were also observed under similar conditions. The $\chi_{mol}T$ vs T plot for [Cu(hfac)$_2$·**D2Py2(TMS)**] is shown in Fig. 11c.

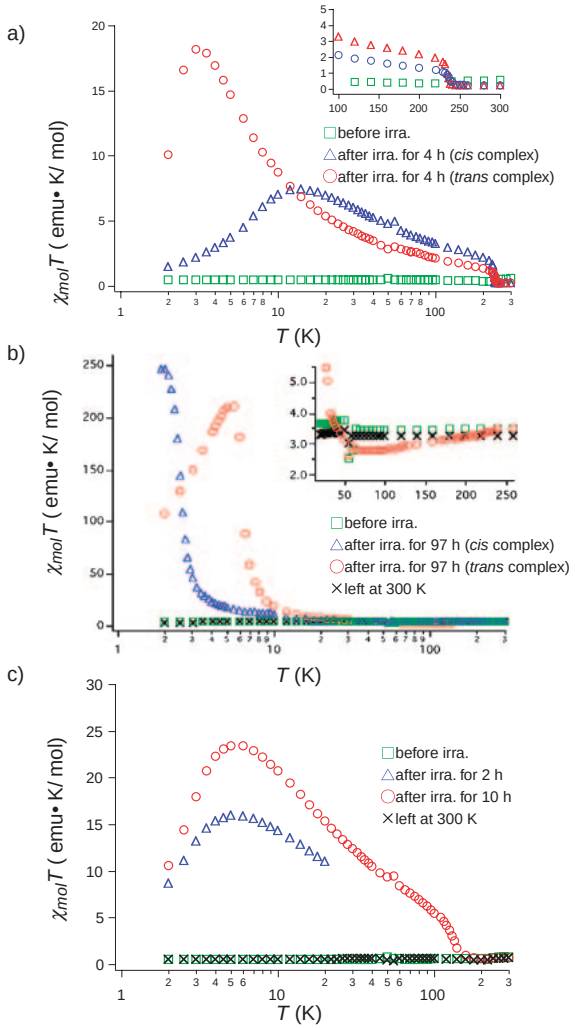

Fig. 11. Temperature dependence of $\chi_{mol}T$ before and after irradiation of a) [Cu(hfac)$_2$•**D1Py2**], b) [Mn(hfac)$_2$•**D1Py2**], and c) [Cu(hfac)$_2$•**D2Py2(TMS)**].

As seen in Fig. 11a and 11b, abrupt changes of the $\chi_{mol}T$ values in $\chi_{mol}T$ vs T plots for [Cu(hfac)$_2$•**D1Py2**] and [Mn(hfac)$_2$•**D1Py2**], were observed at ca. 230 K. The temperature independence of $\chi_{mol}T$ above 230 K and in a consecutive measurement after leaving the sample at 300 K suggested that abrupt change of the $\chi_{mol}T$ values at 230 K was due to the disappearance of the generated carbene centers by chemical reactions. It is worth noting that, whereas the carbene species generated in model complexes [M(hfac)$_2$•(**C1Py**)$_2$] disappeared at 90 K, those in the crystal of [M(hfac)$_2$•**C1Py2**] survived at temperatures as high as 230 K. The observed stability of the carbene centers is novel and most probably due to kinetic protection in the stiff crystal lattice of the metal complex.

The formation of 1D-spin network of 1:1 complexes, [M(hfac)$_2$•**D1Py2** and **D2Py2(TMS)**], can be considered, as shown in Fig. 12, in which the case of the complex **a** for [Cu(hfac)$_2$•**D1Py2**] was described.

PMC, **D1Py2** and **D2Py2(TMS)**, and M(hfac)$_2$ were mixed by 1:1 ratio to form 1D chain structures which were confirmed by X-ray analysis. Before irradiation (a) in Fig. 12 the metal ions in a chain were magnetically isolated and the spins of

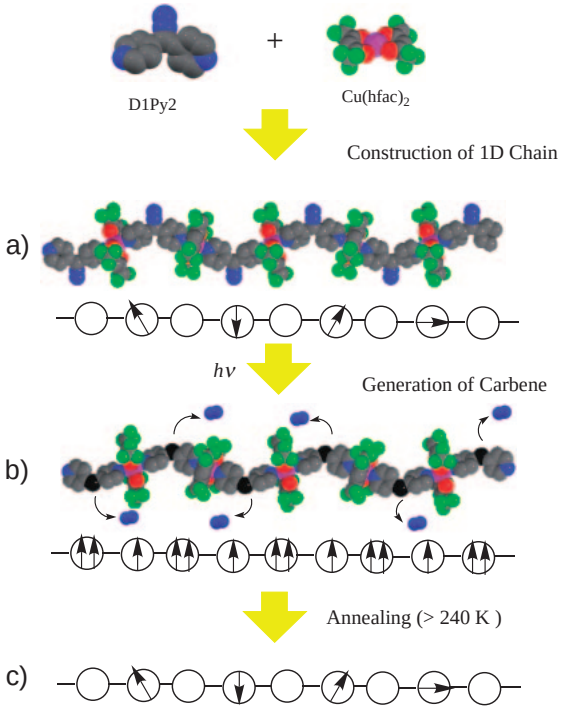

Fig. 12. Photochemical formation of ferromagnetic chain.

metal ion aligned at random. When irradiation started (b) in Fig. 12 the generated carbene centers interacted with both sides of metal ions; ferro- and antiferromagnetically for copper(II) and manganese(II) complexes, to form ferro- and ferrimagnetic chain. Exactly speaking, the p electron in two electrons of a carbene center interacts. From the peak-top $\chi_{mol}T$ values in $\chi_{mol}T$ vs T plots, we estimate the orderings over ca. 6 and 15 units for the complex **a** and **b** of [Cu(hfac)$_2$•**C1Py2**], respectively; over ca. 186 and 218 units for the complexes **a** and **b** of [Mn(hfac)$_2$•**C1Py2**], respectively; and 7 units in [Cu(hfac)$_2$•**C2Py2(TMS)**], along the chains. These correlation lengths should be taken as minimum estimates, since the peak-top $\chi_{mol}T$ values are strongly affected by the saturation at 50 mT employed for the measurement and by the antiferromagnetic interchain interaction. After annealing above 240 K (c) in Fig. 12, carbene decomposed chemically and the spins of the metal ion returned back to being random. The success of the construction of the 1D-spin network proves that our strategy using the heterospin systems is correctly directed toward the molecule-based magnets having a high dimensional spin network.

3. Attempts at 2D- and/or 3D-Spin Networks in Heterospin System

As shown in 3) of Scheme 3, three approaches to 2D- and/or 3D-spin networks can be considered. For approach a) of Scheme 3, a combination of linear diazo dipyridyl PMC, **DXPy2**, and Cu(X)$_2$ was employed at 2:1 ratio. For approach b) and c) in Scheme 3, two highly branched PMCs: tridiazo tripyridyl derivative, **D3Py3**, and pentadiazo tetrapyridyl derivative, **D5Py4**, were designed and prepared (Chart 4).

Carbenes, **C3Py3** and **C5Py4**, generated by photolysis of corresponding diazo compounds were confirmed to be a ground state septet ($S = 6/2$) and undecet ($S = 10/2$), respec-

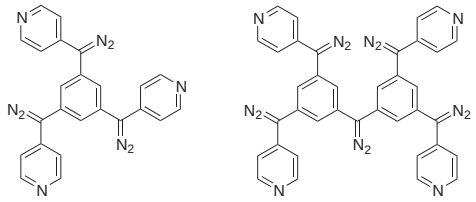

Chart 4. Branched PMCs.

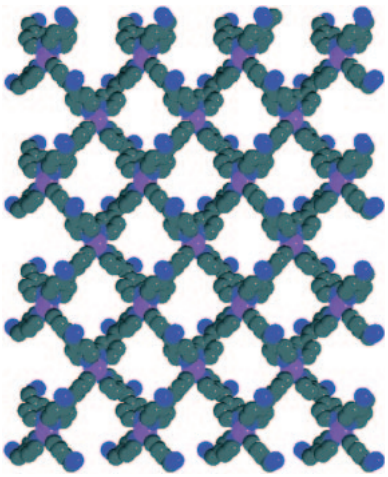

Fig. 13. Crystal structures of $[Cu(NO_3)_2 \cdot (\mathbf{D1Py2})_2]_n$.

tively, by EPR spectrum and magnetization measurements under the conditions similar to the ones for the following experiments on the complex. Each carbene center was also expected to interact ferromagnetically with copper(II) ions through the pyridine rings in the complex with $Cu(hfac)_2$ as described in section **1**.[26,31]

All attempts aiming at the construction of 2D and 3D spin networks are still continuing. At the present stage, only a 2:1 complex of $Cu(NO_3)_2$ with **D1Py2** has been obtained as a single crystal. The crystal structure of $[Cu(NO_3)_2 \cdot (\mathbf{D1Py2})_2]_n$ revealed by a preliminary X-ray analysis has a 2D structure as expected.[32] A CPK model of $[Cu(NO_3)_2 \cdot (\mathbf{D1Py2})_2]_n$ is shown in Fig. 13.

Photolysis of a crystal sample of $[Cu(NO_3)_2 \cdot (\mathbf{D1Py2})_2]_n$ was performed under the conditions similar to those for the 1D chain described in section **3**. However, until now an effective photolysis has not been accomplished. The improvements of our irradiation system and photolysis condition are in progress. In the spin system (b) in 3 of Scheme 3 consisting of $M(hfac)_2$ and branched PMCs, on the other hand, assemblies showing interesting magnetic behavior were found in frozen solution.

4. Heterospin Assemblies Formed in Frozen Solution Condition[33–35]

When the solutions of $Cu(hfac)_2$ and PMC having two or more pyridine units in MTHF were mixed in appropriate ratios, assemblies were expected to form in frozen solution and to show the magnetic behavior that depended on the structure after irradiation. The solutions of $Cu(hfac)_2$ in MTHF and

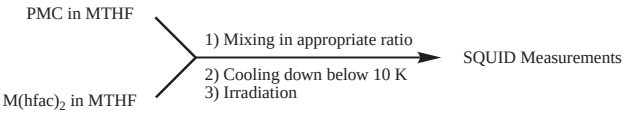

Scheme 5. Experimental procedure for frozen-solution sample.

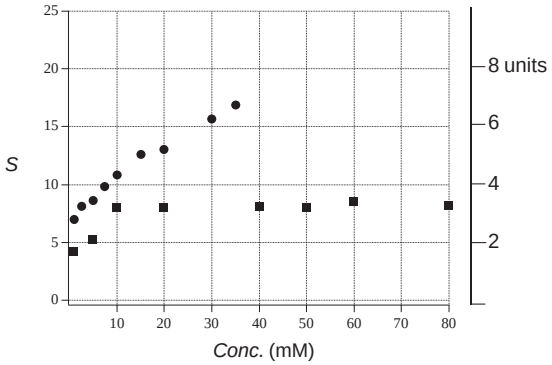

Fig. 14. Plot of spin quantum number, S vs concentration for 1:1 mixture of $Cu(hfac)_2$-**D2Py2(Br)** (●) and $Cu(hfac)_2$-**D2Py2(C_6)** (■) in frozen solution.

PMC in MTHF mixed in appropriate ratios were prepared as samples for a SQUID measurement. The experimental procedure is given in Scheme 5.

4.1 Magnetic Properties of Assemblies Consisting of $Cu(hfac)_2$ with D2Py2(Br) and D2Py2(C_6) in Frozen Solution. First, the field dependence of the magnetization, M, before and after irradiation of the 1:1 mixture samples of $Cu(hfac)_2$ with **D2Py2(Br)** and **D2Py2(C_6)** in various concentrations were measured at 2 K in the field range of 0–50 kOe.[33] Obtained magnetization data in the M vs H plots were analyzed by Brillouin function to afford the spin quantum numbers, S in the ground state. The estimated S values for assemblies of $Cu(hfac)_2$-**D2Py2(Br)** and -**D2Py2(C_6)** formed in frozen solution were plotted as a function of the concentration (Fig. 14).

In $Cu(hfac)_2$-**D2Py2(Br)** assembly, the S value increased linearly with increasing the concentration. On the contrary, the S value for $Cu(hfac)_2$-**D2Py2(C_6)** become constant above 10 mM concentration. The concentration effects of the S values observed for $Cu(hfac)_2$-**D2Py2(Br)** and -**D2Py2(C_6)** may suggest that assemblies formed in frozen solution have a linear chain and a cyclic structure, respectively, above 10 mM. Actually, from $Cu(hfac)_2$-**D2Py2(Br)** solution, the crystal of the complex $[Cu(hfac)_2 \cdot \mathbf{D2Py2(Br)}]_n$ having a linear chain structure was obtained; this was revealed by X-ray structure analysis (Fig. 10c). Although no single crystal from $Cu(hfac)_2$-**D2Py2(C_6)** solution was obtained, on the other hand, if one judges from S values of 18/2–19/2 above 10 mM, which is close to the one (20/2) for the tetramer, the assembly for $Cu(hfac)_2$-**D2Py2(C_6)** might be expected to have a cyclic tetramer structure in Fig. 15a.

4.2 Magnetic Properties of Assemblies Consisting of $Cu(hfac)_2$ with D3Py3 and D5Py4 in Frozen Solution. (A) Dc Magnetic Susceptibility Measurements: In the 3:2 mixtures of $Cu(hfac)_2$ with **D3Py3**,[34] and the 2:1 mixture of $Cu(hfac)_2$ and **D5Py4**,[35] magnetization, M_{mol}, measure-

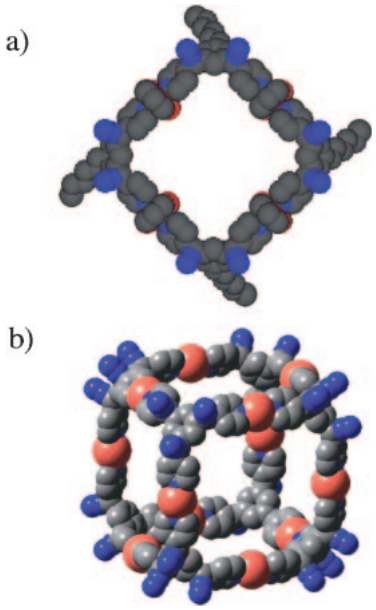

Fig. 15. Plausible tetramer structures of a) Cu(hfac)$_2$-**D2Py2(C$_6$)** and b) [Cu(hfac)$_2$]$_3$-(**D3Py3**)$_2$.

ments before and after irradiation of both samples in various concentrations were also carried out at 2 K under similar conditions. The field-dependence profile of M_{mol} values after irradiation strongly depended on the concentration. The M_{mol} vs H plots at 2 K after irradiation of the 3:2 mixtures of Cu(hfac)$_2$ with **D3Py3** in various concentrations are shown in Fig. 16, together with the results of the 2:1 mixture (1.25 mM) of Cu(hfac)$_2$ and **D5Py4** obtained under similar conditions.

In the 3:2 mixtures of Cu(hfac)$_2$ with **D3Py3**, the magnetization curves were analyzed to consist at least of two components, the fast and slow saturating fractions (FF and SF, respectively). The amounts of FF observed in the low field region (<40 Oe) depended on the concentration of the complex. Furthermore, it is worth noting that the curvature of SF seems to be constant ($S = \sim 52/2$–$60/2$), suggesting that an assembly having single structure might be mainly produced in frozen solution. The constant S value of 26–30 is also close to the one (60/22) for a tetramer of 3:2 complex unit, suggesting the formation of a cubic structure for SF component (a) in Fig. 16. This tetramer might aggregate in high concentration to form FF components exhibiting a spin-glass-like magnetic behavior, which was shown as follows. The sample of 2:1 mixtures of Cu(hfac)$_2$ with **D5Py4** in 1.25 mM also showed steep increase of M_{mol} value in low field region. In both samples, weak hysteresis of M with respect to H were observed; the coercive force and the remnant magnetization for 3:2 mixture and 2:1 mixture were ca. 2 and 2 Oe and 6.3×10^3 and 2.9×10^3 emu·Oe·mol^{-1}, respectively. The large difference between the 3:2 mixture and the 2:1 mixture is that FF was observed in much smaller concentration (~10 times smaller); in 1.25 mM of the 3:2 mixture of Cu(hfac)$_2$ and **D3Py3**, FF was not detectable.

The temperature dependences of the molar paramagnetic susceptibility, χ_{mol} for the samples of 3:2 mixture (20 mM) of Cu(hfac)$_2$ with D3Py3 and the 2:1 mixture (1.25 mM) of Cu(hfac)$_2$ with **D5Py4** in the range of 2–30 K were measured

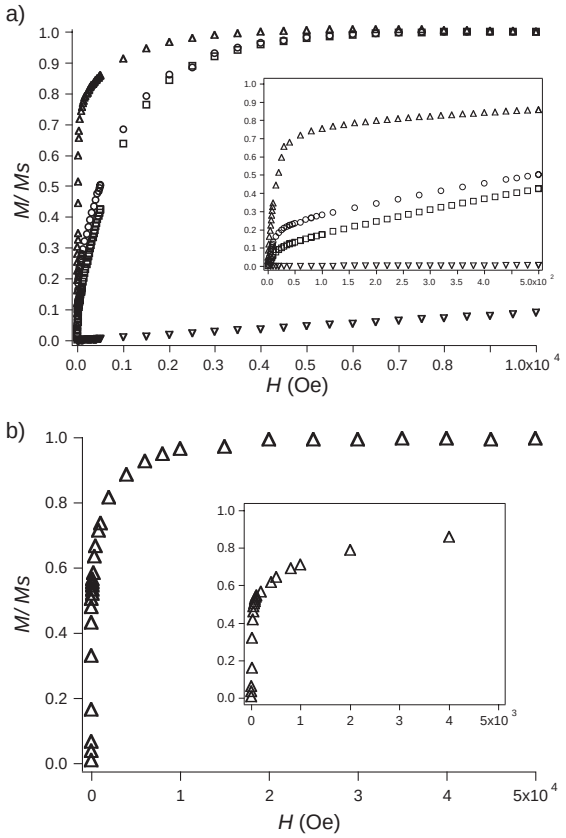

Fig. 16. M/Ms vs H plots at 2 K after irradiation of a) 3:2 mixtures of Cu(hfac)$_2$ with **D3Py3** in 5 (□), 10 (○), and 20 (△) mM concentrations, b) 2:1 mixtures of Cu(hfac)$_2$ with **D5Py4** in 1.25 (△) mM concentrations in frozen solutions. The low-field region (<0.5 kOe) is enlarged in the inset.

at a constant field of 2 Oe. The $\chi_{mol}T$ vs T plots are shown in Fig. 17.

In the 3:2 mixtures of Cu(hfac)$_2$ with **D3Py3**, the χ_{mol} value at 20 K amounted to 143 emu·K·mol^{-1}, which was slightly greater than 116 emu·K·mol^{-1} for a tetramer of [{Cu(hfac)$_2$}$_3$·**C3Py3**)$_2$]. As the temperature was decreased, the χ_{mol} value gradually increased in the range 20–12 K, then steeply increased, reached a maximum of 2.79×10^4 emu·K·mol^{-1} at 9 K, and finally decreased. The observed gradual and steep developments of χ_{mol} value on cooling from 30 K may indicate a ferromagnetic interaction (30–15 K) between the carbene centers and copper(II) ions within the assemblies and a magnetic phase transition (<12 K), respectively. In the 2:1 mixtures of Cu(hfac)$_2$ with **D5Py4**, a similar $\chi_{mol}T$ vs T plot was obtained. The maximum value of χ_{mol} is 2.89×10^3 at 10 K, which corresponds to 564 units of [{Cu(hfac)$_2$}$_2$·**D5Py4**].

(B) Ac Magnetic Susceptibility Measurements: In order to understand the magnetic properties in more detail, ac magnetic susceptibility data for both samples were collected in the temperature range 4.5–15 K with a 1 Oe ac field oscillating at the frequency of 1–750 Hz with a zero dc field. In ac magnetic susceptibility of both samples, the in-phase and out-of-phase components, χ'_{mol} and χ''_{mol}, with frequency dependence were clearly observed, indicating that assemblies in both sam-

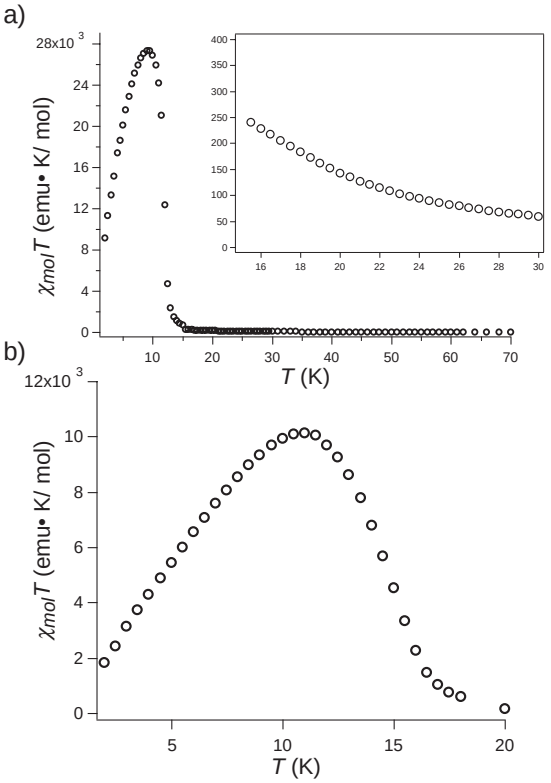

Fig. 17. Temperature dependence of χ_{mol} values after irradiation of samples of a) 3:2 mixture (20 mM, ○) of $Cu(hfac)_2$ with **D3Py3** and b) 2:1 mixture (1.25 mM, ○) of $Cu(hfac)_2$ with **D5Py4** in a frozen solution.

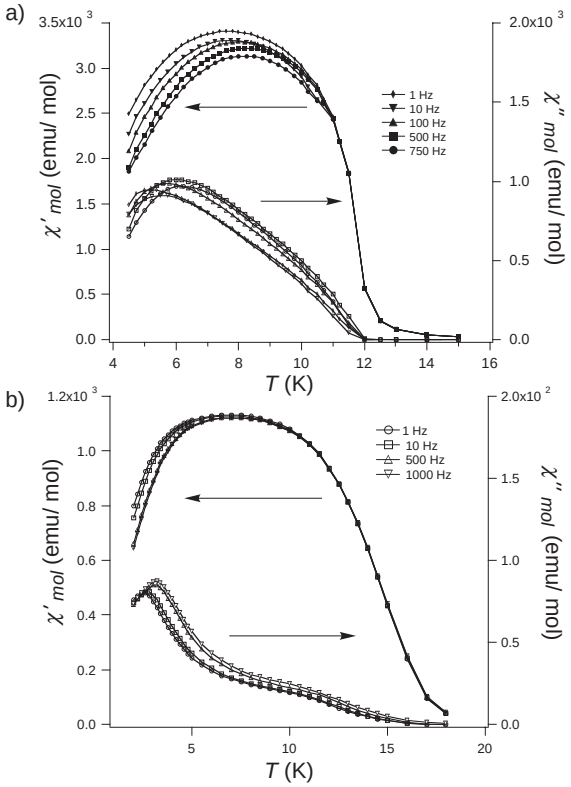

Fig. 18. Temperature dependences of χ'_{mol} and χ''_{mol} after irradiation of a) 3:2 mixture (20 mM) of $Cu(hfac)_2$ with **D3Py3** and b) 2:1 mixture (1.25 mM) of $Cu(hfac)_2$ with **D5Py4** in a frozen solution with a 1 Oe ac field oscillating (zero applied dc field) at various frequencies. Arrows indicate the χ'_{mol} and χ''_{mol} axes.

ple have slow magnetic relaxations. The temperature dependences of χ'_{mol} and χ''_{mol} components for both samples are shown in Fig. 18.

As shown in Fig. 18, plots of χ'_{mol} vs T and χ''_{mol} vs T for both samples are similar to each other and revealed relatively large round maxima. Their peak-top temperature depended on the frequency of applied ac field; the temperature of the round maxima for χ'_{mol} and χ''_{mol} (8.4–7.6 and 6.2–5.2 K, respectively, for 3:2 mixture sample and 7.5–6.5 and 3.2–2.4 K, respectively, for 2:1 mixture sample) decreased, as the field alternation frequency decreased from 750 to 1 Hz. As observed in χ''_{mol} vs T plots, the χ''_{mol} signal showed plural maxima, especially in the 2:1 mixture sample of $Cu(hfac)_2$ with **D5Py4**, indicating that various assemblies might be formed under the experimental conditions. The values of $\Delta T_f/T_f(0)\Delta(\log w)$ obtained from the χ'_{mol} vs T plot, where ΔT_f is the shift of the peak-temperature in χ'_{mol}, $\log w$ is the logarithm of the applied frequency, and $T_f(0)$ is the position of the peak at zero frequency, are 0.04 and 0.056 for 3:2 and 2:1 mixture samples, respectively. According to Mydosh,[36] the values, 0.04 and 0.056, are in the spin-glass region. The observed frequency dependence of χ'_{mol} and χ''_{mol} corresponds better to a spin-glass-like response. The spin-glass-like magnetic behaviors observed in the dc and ac magnetic susceptibility measurements for both samples were reproducible below 20 K.

The magnetic behavior after photolysis of self-assemblies formed in the frozen solution strongly depends on the structure of the photoresponsive magnetic coupler. As discussed in section **3**, no FF was observed in a combination of $Cu(hfac)_2$ and **D2Py2** which has a partial structure of **D3Py3**, under the condition similar to this work; they showed an increase of average S values (8–17) in proportion to the concentration in the range of 1.0–35 mM. Although it is very difficult to reveal the structure of the self-assemblies formed in frozen solution, we took advantage of our heterospin system and could successfully construct assemblies having spin-glass-like magnetic properties by the simple procedure of mixing the two components in solutions and freezing them below 30 K, followed by irradiation. Now, to obtain the information related to the size and shape of an assembly formed in frozen solution, the study by means of a small angle neutron scattering (SANS) was started. The construction of the spin-glass reported here suggests a new approach to the single-molecule magnets by employing anisotropic metal ions in place of copper(II) ions.

5. Formation of Single-Molecule Magnet (SMM) in Frozen Solution[37,38]

To gain the large $|D|S^2$ value required for SMM, we took advantage of our heterospin system in which the metal ions and the organic spins contribute to large D values and large S values, respectively. As SMM belongs to 0D spin network with an Ising type anisotropy, the two approaches which are shown in a) and b) of 1) of Scheme 3 were considered for

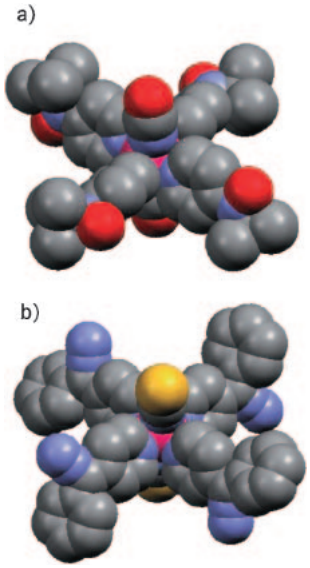

Fig. 19. Molecular structures of a) $[Co(NCO)_2 \cdot (\mathbf{4NOPy})_4]$ and b) $[Co(NCS)_2 \cdot (\mathbf{D1Py})_4]$.

the construction of SMM. A salicylaldehyde Schiff-base cobalt(II) complex, Co(*p*-tolsal)$_2$,[39] and Co(L)$_2$; L = NCS, NCO, Br, Cl, for the former and the latter approaches, respectively, were selected as metal ion. A high-spin cobalt(II) ion or complex is known to have a relatively large magnetic anisotropy and is often employed for SMM. Monopyridine derivatives carrying organic spin, **4NOPy** and **C1Py**, were selected. In this paper, only approach b) in Scheme 3 will be reported.

5.1 Molecular Structures of Monometallic SMMs. Crystalline complexes, $[Co(L)_2 \cdot (\mathbf{4NOPy})_4]$ and $[Co(L)_2 \cdot (\mathbf{D1Py})_4]$, were obtained by mixing the solution of appropriate cobalt(II) salt (CoL_2; L = NCS, NCO, Br, Cl) and the solution of monopyridine ligands (**4NOPy** and **D1Py**) in 1:4 ratios. Their molecular structures revealed by X-ray analysis are compressed octahedrals in which the axial ligand ions are coordinated in relatively short distances by *trans* configuration. The molecular structures of $[Co(NCO)_2 \cdot (\mathbf{4NOPy})_4]$[37] and $[Co(NCS)_2 \cdot (\mathbf{D1Py})_4]$[38] are shown in Figs. 19a and 19b, respectively.

Magnetic properties of a 1:4 mixture of Co(X)$_2$ and **4NOPy** (or **C1Py**) in a frozen solution were investigated by SQUID magneto/susceptometry. Before magnetic experiment in frozen solution, we confirmed by the temperature dependence of Vis–NIR spectra that the 1:4 mixture of Co(L)$_2$ and **4NOPy** (or **D1Py**) in frozen solution can safely be considered to be the octahedral complex having the structure shown in Fig. 19. Vis–NIR spectra changes for $[Co(NCO)_2 \cdot (\mathbf{4NOPy})_4]$ in MTHF solution in the temperature range of 295–160 K are shown in Fig. 20. The spectra at 295 and 160 K are characteristic to a cobalt(II) complex having the tetrahedral and octahedral structure, respectively.

5.2 Magnetic Properties of Monometallic SMMs. (A) Ac Magnetic Susceptibility Measurements: The ac magnetic susceptibility data for a frozen-solution sample of $[Co(NCO)_2 \cdot (\mathbf{4NOPy})_4]$ were measured in a zero dc field with a 5.0 Oe ac field and in the temperature range of 1.9–10 K. In the complex, well-resolved χ'_{mol} and χ''_{mol} signals (in-phase and out-of-phase components of ac magnetic susceptibilities,

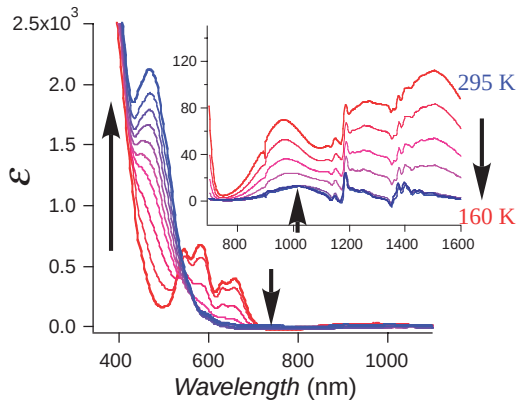

Fig. 20. Vis–NIR spectra changes for $[Co(NCO)_2 \cdot (\mathbf{4NOPy})_4]$ in MTHF solution in the temperature range of 295–160 K.

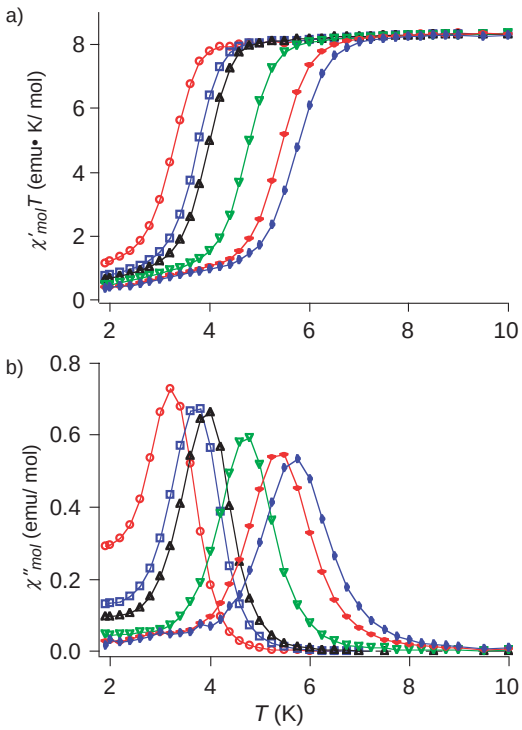

Fig. 21. Plots of a) $\chi'_{mol}T$ vs T and b) χ''_{mol} vs T of a 1:4 mixture (10 mM) of $Co(NCO)_2$ and **4NOPy** in frozen MTHF solution with a 5 Oe ac field oscillating at 1000 (◆), 500 (◆), 100 (▽), 10 (△), 5 (□), and 1 (○) Hz. The solid lines are visual guides.

respectively) with the frequency dependence were observed, indicating that the complex has a slow magnetic relaxation for flipping the spin. In the $\chi'_{mol}T$ vs T plots (Fig. 21a), the values of $\chi'_{mol}T$ were nearly constant (8.7–8.5 emu·K·mol^{-1}) until the onset of the contribution of out-of-phase χ''_{mol} signals. The value of 8.5 emu·K·mol^{-1} is much larger than the one (3.5) calculated by spin-only equation with four isolated aminoxyls (0.375×4) and one high-spin cobalt(II) ion (2.0×1), suggesting that the aminoxyl and the cobalt ion in the complex interacted ferromagnetically to form the high-spin ground state with $S = 5/2$ and $g = 2.8$ (assuming the effective

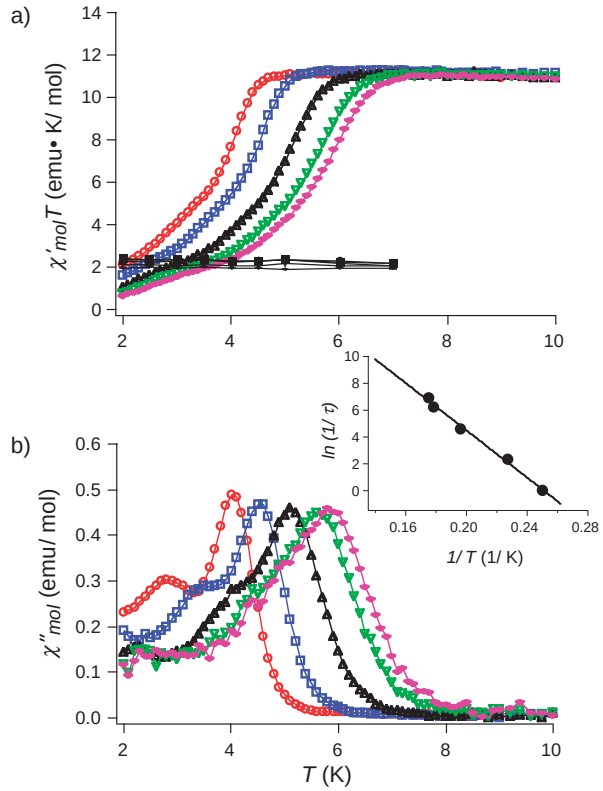

Fig. 22. Plots of a) $\chi'_{mol}T$ vs T and b) χ''_{mol} vs T obtained after irradiation of a 1:4 mixture (10 mM) of $Co(NCS)_2$ and **D1Py** in frozen MTHF–EtOH solution with a 5 Oe ac field oscillating at 1000 (◆), 500 (▽), 100 (△), 10 (□), and 1 (○) Hz. The solid lines are visual guides. The black filled marks in a) are the data before irradiation and the inset in b) is an Arrhenius plot for the component A.

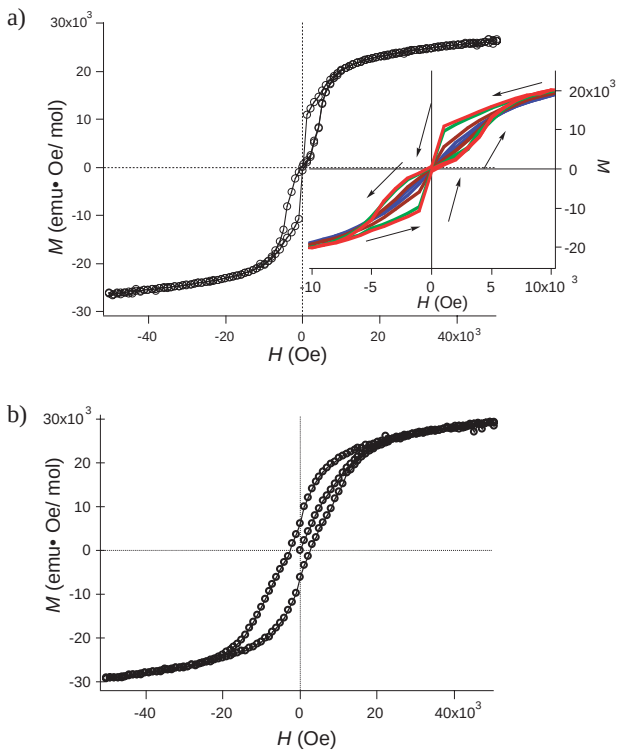

Fig. 23. Plot of a hysteresis loop obtained at 2 K of a 1:4 mixture of $Co(NCO)_2$ and **4NOPy** in frozen MTHF solution (a) and at 2 K after irradiation of a 1:4 mixture of $Co(NCS)_2$ and **D1Py** in frozen MTHF–EtOH solution (b) with a sweeping rate of 0.35 kOe/sec.

$S' = 1/2$ for cobalt(II) ion which was obtained by EPR study on $[Co(NCS)_2 \cdot (Py)_4]$). As observed in the χ''_{mol}–T plot (Fig. 21b), χ''_{mol} signals at each frequency showed a maximum above 1.9 K and the peak-top temperature shifted to lower values as the frequency decreased. In addition to the main peak, a small peak (shoulder) due to a minor component formed under the experimental conditions was observed in the lower temperature region. Since each frequency at the peak-top temperature for χ''_{mol} is consistent with $1/\tau$, the activation energy, Δ/k_B, for flipping the spin and the relaxation time, τ_0, were estimated from the Arrhenius plot: $\tau = \tau_0 \exp(\Delta/k_B T)$ to give $\Delta/k_B = 50$ K and $\tau_0 = 1.8 \times 10^{-7}$ sec. Similar magnetic behavior showing slow magnetic relaxation was observed in a frozen-solution sample of $[Co(NCS)_2 \cdot (\mathbf{4NOPy})_4]$ under similar conditions: $\Delta/k_B = 30$ K. This result is worthy to note: the activation barrier for flipping the spin in these spin systems can be controlled by the axial ligands.

Ac magnetic susceptibility measurements for 1:4 mixture of $Co(NCS)_2$ and **D1Py** (10 mM/50 mL) in MTHF–EtOH were performed under similar conditions. Before irradiation, no magnetic behavior of the slow spin relaxation was observed. After irradiation for 30 h, on the other hand, both in-phase and out-of-phase components, χ'_{mol} and χ''_{mol}, respectively, of the ac magnetic susceptibility showed frequency dependence. The plots of $\chi'_{mol}T$ vs T and χ''_{mol} vs T before and after irradiation are shown in Figs. 22a and b, respectively.

As one can observe in Fig. 21b, the signals due to χ''_{mol} showed two maxima at each frequency. Especially, two maxima were clearly observed in 1 Hz signals at 2.8 and 4.0 K. This double relaxation suggested the presence of two components (A and B in which Δ/k_B for A is larger) under the experimental conditions. From each frequency at the peak-top temperature for χ''_{mol}, the activation energy, Δ/k_B, for flipping the spin and the relaxation time, τ_0, were obtained; $\Delta/k_B = 89$ (50) K and $\tau_0 = 2.3 \times 10^{-10}$ (3.2×10^{-10}) sec. The values in parentheses are for component B.

(B) Dc Magnetic Susceptibility Measurements: A magnetization hysteresis loop of the frozen solution sample of $[Co(NCO)_2 \cdot (\mathbf{4NOPy})_4]$ was also measured with a sweep rate of 0.35 kOe/sec at five temperatures in the range 1.9–3.0 K (Fig. 23a). The hysteresis loop appeared below ca. 2.5 K and the area within the loop increased with decreasing temperature. The M_{mol} value sigmoidally increased in the range of 0–5 kOe on applying field from 0 to 50 kOe and abruptly decreased near zero Oe on reducing the field from 50 to 0 kOe (the inset of Fig. 23a). In a negative field, a similar behavior of the M_{mol} value was observed with the negative sign. The shape of the observed hysteresis loop might be due to a fast magnetization relaxation at zero Oe and the effect of minor component(s) contained under experimental conditions. Taking the result of ac experiments into account, however, the contribution of

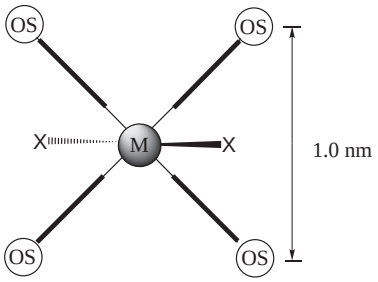

Scheme 6. Shape and size of heterospin system in [Co(NCO)$_2$·(**4NOPy**)$_4$] and [Co(NCS)$_2$·(**C1Py**)$_4$].

the latter might be small.

The dc magnetization for [Co(NCS)$_2$·(**C1Py**)$_4$] was also measured under similar conditions. The cobalt complex exhibited a hysteresis with respect to the applied field below ca. 3.5 K; the hysteresis loops increased with decreasing temperature. Coercive force and remnant magnetization at 2 K are ca. 3.0 kOe and 6.5×10^3 emu·Oe·mol^{-1}, respectively.

The decays of magnetization for [Co(NCS)$_2$·(**C1Py**)$_4$] were followed after the cycles of applying 10 kOe and then reducing to the zero field. Dc magnetization decay data were collected at 9 temperatures in the 3.4–1.9 K and analyzed by the extended exponential equation. The rates of dc magnetization decay which are ca. 2×10^{-3} sec^{-1}, are nearly constant in the temperature range of 2.7–1.9 K. The observed dc decay might be due to the spin quantum tunneling. When the irradiated sample was annealed at 90 K, the observed dc and ac magnetic signals completely disappeared and the magnetic behavior returned to those before irradiation.

Although it is difficult to obtain any direct information on the structure of [Co(NCO)$_2$·(**4NOPy**)$_4$] and [Co(NCS)$_2$·(**C1Py**)$_4$] formed in frozen solution, the origin of observed magnetic behaviors may be safely concluded to be due to one isolated molecule of the cobalt complex. The lack of concentration dependence, strong frequency dependence of χ' and χ'' signals, and the physically reasonable value of τ_0 for [Co(NCO)$_2$·(**4NOPy**)$_4$] and [Co(NCS)$_2$·(**C1Py**)$_4$] in frozen solution suggest that the Co complex in frozen solution functions rather as an SMM than a spin glass.[40] As illustrated in Scheme 6, these complexes are monometallic SMM which have a nm size.

The combination of the high-spin organic radicals and the magnetically anisotropic metal ions will lead to the development of a new type of single-molecule magnets of a nm size. To understand magnetic properties of SMM in more detail, we are continuing the quantitative and theoretical analyses using [Co(X)$_2$·(**4NOPy**)$_4$] and we are studying the influence of the systematic changes of S values of carbenes by using [Co(NCS)$_2$·(**CXPy**)$_4$].

6. Concluding Remarks

The chemistry of high-spin polycarbenes started from *m*-phenylenedicarbene, **C2**, with a quintet ground state reported by K. Itoh[41] and E. Wasserman[42] in 1967. In the early eighties, tetra-, penta-, and hexa-diazo derivatives ($n = 4$, 5, and 6 in **Dn**)[43] and dendritic polydiazo derivatives (**Dbn**)[44] were systematically prepared and their photoproducts, polycarbene, were confirmed to have high-spin ground states, which were

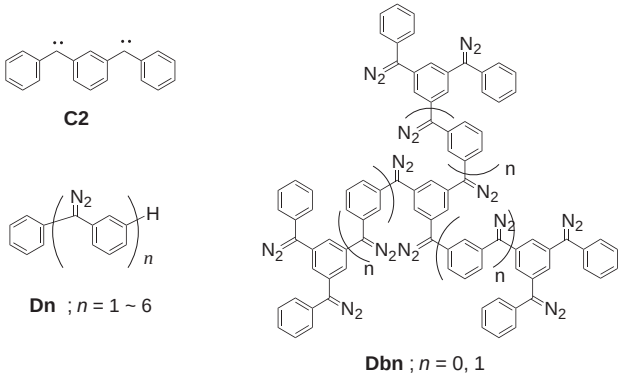

Chart 5. Linear and dendritic polydiazo derivatives.

reported by H. Iwamura (Chart 5). This polycarbene study not only suggested the idea for the construction of pure organic ferromagnets[45] but also gave us valuable magnetic information in the present heterospin system. It is worthy to note that the carbene, which is usually regarded as a reactive intermediate, is considered as a spin source in the study on the magnetism.

Based on the above study of the high-spin hydrocarbon polycarbenes, we worked out a strategy for preparing the molecule-based magnets using a heterospin system consisting of organic 2p spins and metal ions. First of all, to confirm the magnetic coupling between paramagnetic metal ion and organic spin through π-conjugated ligand, we prepared discrete model complexes. Their magnetic studies revealed that the magnetic coupling depended on the magnetic orbital in metal ion and the regiospecificity in the exchange coupling with respect to the aminoxyl radical site on the pyridine ring. The intramolecular magnetic couplings were explained by a spin polarization mechanism. Based on this information, 1D chain spin networks were designed and prepared. In 1:1 complex of M(hfac)$_2$; M = Mn and Cu, and **D1Py2** (or **D2Py2(TMS)**), the formation of ferri- and ferromagnetic chain, respectively, were successfully observed after irradiation. These 1D works were extended to a high-dimensional spin network by using metal ions without diamagnetic ligand such as hfac and branched PMC.

On the other hand, assemblies formed in frozen solution were found to exhibit interesting magnetic behavior. The 3:2 complex of Cu(hfac)$_2$ with **D3Py3** in frozen solution after irradiation showed spin-glass-like magnetic behavior. This finding led to a new approach to SMM in heterospin systems. The 1:4 complexes of CoX$_2$; X = NCO, NCS, and Br, with **4NOPy** in frozen-solution function as SMM with activation barrier for flipping the spin ($\Delta/k_B = 50$–20 K). Analogous cobalt complex using **D1Py** after irradiation showed similar SMM behavior with $\Delta/k_B = 90$ K. These cobalt complexes are the first examples of a monometallic SMM in nanometer size.

In the area of molecule-based magnets, it is widely accepted that the new magnets will never replace conventional magnets made by metals, metal oxides, and alloys, etc. Instead they should have additional functions such as the response to light, pressure, electric current, or pH. Thus, our photoresponsive magnets will reveal the magnetism only in the part exposed to the light and will be expected to act as high-resolution photomagnetic devices in the material science of the next generation.

We are thankful to Professor H. Iwamura for helpful discussions. This work was supported by a Grant-in-Aid for Scientific Research (A)(2)(No. 14204071) from the Ministry of Education, Culture, Sports, Science and Technology, Japan, and by "Nanotechnology Support Project" of the Ministry of Education, Culture, Sports, Science and Technology (MEXT), Japan.

References

1 a) O. Kahn, "Molecular Magnetism," Wiley-VCH, New York (1993). b) O. Kahn, *Nature*, **378**, 667 (1995). c) D. Gatteschi, *Adv. Mater.*, **6**, 635 (1994). d) J. S. Miller, A. J. Epstein, and W. M. Reiff, *Chem. Rev.*, **88**, 201 (1988). e) M. Ohba and H. Okawa, *Coord. Chem. Rev.*, **198**, 313 (2000).

2 O. Sato, T. Iyoda, A. Fujishima, and K. Hashimoto, *Science*, **272**, 704 (1996).

3 D. Gatteschi and R. Sessoli, *Angew. Chem., Int. Ed.*, **42**, 268 (2003).

4 a) S. Wang, J. Zuo, S. Gao, Y. Song, H. Zhou, Y. Zhang, and X. You, *J. Am. Chem. Soc.*, **126**, 8900 (2004). b) H. Miyasaka, R. Clérac, K. Mizushima, K. Sugiura, M. Yamashita, W. Wernsdorfer, and C. Coulon, *Inorg. Chem.*, **42**, 8203 (2003). c) R. Clérac, H. Miyasaka, M. Yamashita, and C. Coulon, *J. Am. Chem. Soc.*, **124**, 12837 (2002). d) A. Caneschi, D. Gatteschi, N. Lalioti, C. Sangregorio, R. Sessoli, G. Venturi, A. Vindigni, A. Rettori, M. G. Pini, and M. A. Novak, *Angew. Chem., Int. Ed.*, **40**, 1760 (2001).

5 a) H. Miyasaka, H. Ieda, N. Masamoto, K. Sugiura, and M. Yamashita, *Inorg. Chem.*, **42**, 3509 (2003). b) J. Larionova, O. Kahn, S. Gohlen, L. Ouahab, and R. Clérac, *J. Am. Chem. Soc.*, **121**, 3349 (1999). c) J. Larionova, O. Kahn, S. Golhen, L. Ouahab, and R. Clérac, *Inorg. Chem.*, **38**, 3621 (1999).

6 N. Koga and H. Iwamura, "Magnetic Properties of Organic Materials," ed by P. Lahti, Marcel Dekker, New York (1999), Chap. 30, p. 629.

7 a) A. Caneschi, D. Gatteschi, and R. Sessoli, *Inorg. Chem.*, **32**, 4612 (1993). b) A. Caneschi, D. Gatteschi, P. Rey, and R. Sessoli, *Inorg. Chem.*, **30**, 3936 (1991). c) A. Caneschi, D. Gatteschi, R. Sessoli, and M. Corti, *J. Am. Chem. Soc.*, **113**, 8410 (1991).

8 a) K. Inoue, T. Hayamizu, H. Iwamura, D. Hashizume, and Y. Ohashi, *J. Am. Chem. Soc.*, **118**, 1803 (1996). b) K. Inoue and H. Iwamura, *Adv. Mater.*, **8**, 73 (1996). c) D. C. Oniciu, K. Matsuda, and H. Iwamura, *J. Chem. Soc., Perkin Trans. 2*, **1996**, 903. d) H. Iwamura, K. Inoue, and T. Hayamizu, *Pure Appl. Chem.*, **68**, 243 (1996). e) K. Inoue and H. Iwamura, *Mater. Res. Soc. Symp. Proc.*, **413**, 313 (1996). f) T. Mitsumori, K. Inoue, N. Koga, and H. Iwamura, *J. Am. Chem. Soc.*, **117**, 2467 (1995). g) K. Inoue and H. Iwamura, *J. Am. Chem. Soc.*, **116**, 3173 (1994).

9 a) J. F. Nierengarten, C. O. Dietrich-Buchecker, and J. P. Sauvage, *J. Am. Chem. Soc.*, **116**, 375 (1994). b) J. M. Lehn, "Supramolecular Chemistry," Wiley-VCH, Weinheim (1995). c) M. Fujita, F. Ibukuro, K. Yamaguchi, and K. Ogura, *J. Am. Chem. Soc.*, **117**, 4175 (1995). d) J. F. Nierengarten, C. O. Dietrich-Buchecker, D. B. Amabilino, and J. F. Stoddart, *Chem. Rev.*, **95**, 2725 (1995). e) S. Leininger, B. Olenyuk, and P. J. Stang, *Chem. Rev.*, **100**, 853 (2000).

10 a) S. Nakazono, S. Karasawa, N. Koga, and H. Iwamura, *Angew. Chem., Int. Ed.*, **37**, 1550 (1998). b) R. Chiarelli, S. Ganbarelli, and A. Rassat, *Mol. Cryst. Liq. Cryst.*, **108**, 455 (1997). c) A. Calder, A. R. Forrester, P. G. James, and G. R. Luckhurst, *J. Am. Chem. Soc.*, **91**, 3724 (1969). d) K. Mukai, H. Nagai, and K. Ishizu, *Bull. Chem. Soc. Jpn.*, **48**, 2381 (1975). e) T. Ishida and H. Iwamura, *J. Am. Chem. Soc.*, **113**, 4238 (1991). f) F. Kanno, K. Inoue, N. Koga, and H. Iwamura, *J. Am. Chem. Soc.*, **115**, 847 (1993).

11 N. Koga and H. Iwamura, "Carbene Chemistry from Fleeting Intermediates to Powerful Reagents," ed by G. Bertrand, Marcel Dekker, New York (2002), Chap. 9, p. 271.

12 a) M. Soler, W. Wernsdorfer, K. A. Abboud, J. C. Huffman, E. R. Davidson, D. N. Hendrickson, and G. Christou, *J. Am. Chem. Soc.*, **125**, 3576 (2003). b) C. Boskovic, E. K. Brechin, W. E. Streib, K. Folting, J. C. Bollinger, D. N. Hendrickson, and G. Christou, *J. Am. Chem. Soc.*, **124**, 3725 (2002). c) L. Thomas, F. Lionti, R. Ballou, D. Gatteschi, R. Sessoli, and B. Barbara, *Nature*, **383**, 145 (1996). d) R. Sessoli, D. Gatteschi, A. Caneschi, and M. A. Novak, *Nature*, **365**, 141 (1993). e) R. Sessoli, H. L. Tsai, A. R. Schake, A. Wang, J. B. Vincent, K. Folting, D. Gatteschi, G. Christou, and D. N. Hendrickson, *J. Am. Chem. Soc.*, **115**, 1804 (1993).

13 S. L. Castro, Z. Sun, C. M. Grant, J. C. Bollinger, D. N. Hendrickson, and G. Christou, *J. Am. Chem. Soc.*, **120**, 2365 (1998).

14 a) C. Boskovic, W. Wensdorfer, K. Foling, J. C. Huffman, D. N. Hendrickson, and G. Christou, *Inorg. Chem.*, **41**, 5107 (2002). b) S. M. J. Aubin, N. R. Dilley, M. W. Wemple, M. B. Maple, G. Christou, and D. N. Hendrickson, *J. Am. Chem. Soc.*, **120**, 839 (1998).

15 a) H. Oshio, N. Hoshino, T. Ito, and M. Nakano, *J. Am. Chem. Soc.*, **126**, 8805 (2004). b) C. Sangregorio, T. Ohm, C. Paulsen, R. Sessoli, and D. Gatteschi, *Phys. Rev. Lett.*, **78**, 4645 (1997).

16 a) M. Murrie, S. J. Teat, H. Stoeckli-Evans, and H. U. Güdel, *Angew. Chem., Int. Ed.*, **42**, 4653 (2003). b) J. R. Galan-Mascaros and K. R. Dunbar, *Angew. Chem., Int. Ed.*, **42**, 2289 (2003). c) E. C. Yang, D. N. Hendrickson, W. Wernsdorfer, M. Nakano, L. N. Zakharov, R. D. Sommer, A. L. Rheingold, M. Ledezma-Gaeraud, and G. Christou, *J. Appl. Phys.*, **91**, 7382 (2002). d) A. Caneschi, D. Gatteschi, N. Lalioti, R. Sessoli, L. Sorace, V. Tangoulis, and A. Vindigni, *Chem.—Eur. J.*, **8**, 286 (2002).

17 H. Andres, R. Basler, A. J. Blake, C. Cadiou, G. Chaboussant, C. M. Grant, H. U. Güdel, M. Murrie, S. Parsons, C. Paulsen, F. Semadini, V. Villar, W. Wernsdorfer, and R. E. P. Winpenny, *Chem.—Eur. J.*, **8**, 4867 (2002).

18 a) S. Osa, T. Kido, N. Matsumoto, N. Re, A. Pochaba, and J. Mrozinski, *J. Am. Chem. Soc.*, **126**, 420 (2004). b) N. Ishikawa, M. Sugita, T. Ishikawa, S. Koshihara, and Y. Kaizu, *J. Am. Chem. Soc.*, **125**, 8694 (2003).

19 M. Kitano, Y. Ishimaru, K. Inoue, N. Koga, and H. Iwamura, *Inorg. Chem.*, **33**, 6012 (1994).

20 S. Karasawa and N. Koga, unpublished result.

21 Y. Ishimaru, M. Kitano, H. Kumada, N. Koga, and H. Iwamura, *Inorg. Chem.*, **37**, 2273 (1998).

22 Y. Ishimaru, K. Inoue, N. Koga, and H. Iwamura, *Chem. Lett.*, **1994**, 1693.

23 H. Kumada, A. Sakane, N. Koga, and H. Iwamura, *J. Chem. Soc., Dalton Trans.*, **2000**, 911.

24 A. Sakane, H. Kumada, S. Karasawa, N. Koga, and H. Iwamura, *Inorg. Chem.*, **39**, 2891 (2000).

25 N. Koga, Y. Ishimaru, and H. Iwamura, *Angew. Chem., Int. Ed. Engl.*, **35**, 755 (1996).

26 a) Y. Sano, M. Tanaka, N. Koga, K. Matsuda, H. Iwamura,

P. Rabu, and M. Drillon, *J. Am. Chem. Soc.*, **119**, 8246 (1997). b) N. Koga and H. Iwamura, *Mol. Cryst. Liq. Cryst.*, **305**, 415 (1997).

27 H. Morikawa, F. Imamura, Y. Tsurukami, T. Itoh, H. Kumada, S. Karasawa, N. Koga, and H. Iwamura, *J. Mater. Chem.*, **11**, 493 (2001).

28 M. Kitano, N. Koga, and H. Iwamura, *J. Chem. Soc., Chem. Commun.*, **1994**, 447.

29 D. Luneau, P. Rey, J. Laugier, P. Fries, A. Caneschi, D. Gatteschi, and R. Sessoli, *J. Am. Chem. Soc.*, **113**, 1245 (1991).

30 S. Karasawa, Y. Sano, T. Akita, N. Koga, T. Itoh, H. Iwamura, P. Rabu, and M. Drillon, *J. Am. Chem. Soc.*, **120**, 10080 (1998).

31 S. Karasawa, M. Tanaka, N. Koga, and H. Iwamura, *J. Chem. Soc., Chem. Commun.*, **1997**, 1359.

32 T. Itoh and N. Koga, unpublished result.

33 Y. Tsurukami, S. Karasawa, and N. Koga, to be published elsewhere.

34 a) S. Karasawa, H. Kumada, N. Koga, and H. Iwamura, *J. Am. Chem. Soc.*, **123**, 9685 (2001). b) S. Karasawa and N. Koga, *Polyhedron*, **20**, 1387 (2001).

35 S. Karasawa and N. Koga, *Polyhedron*, **22**, 1877 (2003).

36 J. A. Mydosh, "Spin Glasses; An Experimental Introduction," Taylor and Francis, London (1993).

37 S. Kanegawa, S. Karasawa, M. Nakano, and N. Koga, *J. Chem. Soc., Chem. Commun.*, **2004**, 1750.

38 S. Karasawa, G. Zhou, H. Morikawa, and N. Koga, *J. Am. Chem. Soc.*, **125**, 13676 (2003).

39 a) D. A. House and N. F. Curtis, *J. Am. Chem. Soc.*, **84**, 3248 (1962). b) N. Yamamoto, J. Tanokashira, S. Karasawa, and N. Koga, to be published elsewhere.

40 a) M. A. Gîrtu, C. M. Wynn, W. Fujita, K. Awaga, and A. J. Epstein, *Phy. Rev. B*, **61**, 4117 (2000). b) S. P. Sellers, B. J. Korte, J. P. Fitzgerald, W. M. Reiff, and G. Yee, *J. Am. Chem. Soc.*, **120**, 4662 (1998). c) J. E. Greedan, N. P. Raju, A. Maignan, Ch. Simon, J. S. Pedersen, A. M. Niraimathi, E. Gmelin, and M. A. Subramanian, *Phy. Rev. B*, **54**, 7189 (1996).

41 K. Itoh, *Chem. Phys. Lett.*, **1**, 235 (1967).

42 E. Wasserman, R. W. Murray, W. A. Yager, A. M. Trozzolo, and G. Smolinsky, *J. Am. Chem. Soc.*, **80**, 5076 (1967).

43 a) Y. Teki, T. Takui, K. Itoh, H. Iwamura, and K. Kobayashi, *J. Am. Chem. Soc.*, **108**, 2147 (1986). b) A. Izuoka, S. Murata, T. Sugawara, and H. Iwamura, *J. Am. Chem. Soc.*, **109**, 2631 (1987). c) N. Koga and H. Iwamura, *Nippon Kagaku Kaishi*, **1989**, 1456. d) I. Fujita, Y. Teki, T. Takui, T. Kinoshita, K. Itoh, F. Miko, Y. Sawaki, H. Iwamura, A. Izuoka, and T. Sugawara, *J. Am. Chem. Soc.*, **112**, 4074 (1990). e) N. Nakamura, K. Inoue, H. Iwamura, T. Fujioka, and Y. Sawaki, *J. Am. Chem. Soc.*, **114**, 1484 (1992).

44 a) K. Matsuda, N. Nakamura, K. Inoue, N. Koga, and H. Iwamura, *Bull. Chem. Soc. Jpn.*, **69**, 1483 (1996). b) K. Matsuda, N. Nakamura, K. Inoue, N. Koga, and H. Iwamura, *Chem.—Eur. J.*, **2**, 259 (1996). c) K. Matsuda, N. Nakamura, K. Takahashi, K. Inoue, N. Koga, and H. Iwamura, *J. Am. Chem. Soc.*, **11**, 5550 (1995). d) N. Nakamura, K. Inoue, and H. Iwamura, *Angew. Chem., Int. Ed. Engl.*, **32**, 872 (1993).

45 a) M. Kinoshita, P. Turek, M. Tamura, K. Nozawa, D. Shiomi, Y. Nakazawa, M. Ishikawa, M. Takahashi, K. Awaga, T. Inabe, and Y. Maruyama, *Chem. Lett.*, **1991**, 1225. b) W. Fujita and K. Awaga, *Chem. Phys. Lett.*, **388**, 186 (2004). c) A. Alberola, R. J. Less, C. M. Pask, J. M. Rawson, F. Palacio, P. Oliete, C. Paulsen, A. Yamaguchi, R. D. Farley, and D. M. Murphy, *Angew. Chem., Int. Ed.*, **42**, 4782 (2003). d) M. Matsushita, A. Izuoka, T. Sugawara, T. Kobayashi, N. Wada, N. Takeda, and M. Ishikawa, *J. Am. Chem. Soc.*, **119**, 4369 (1997).

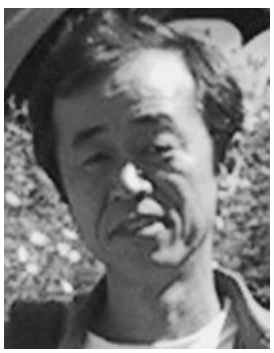

Noboru Koga was born in Sasebo in 1950. He graduated from the Faculty of Pharmaceutical Sciences of Kyushu University in 1974. He received the M. Phar. (1976) and the Ph.D. (1979) from Kyushu University. He worked with Professor T. G. Traylor at UC, San Diego (U. S. A.), as a postdoctoral fellow in 1979–1982. He was pointed as a research associate at Institute for Molecular Science in 1982, moved to the Faculty of Science, The University of Tokyo, in 1988, and then was promoted as an associate professor in 1992. Since 1995, he has been a professor of Pharmaceutical Science at Kyushu University. One of his current subjects is the approaches to molecule-based magnets from the field of physical organic chemistry.

Satoru Karasawa was born in Nagano Prefecture in 1971. He graduated from the Department of Pharmacy of Meiji Pharmaceutical University in 1994. He received the M. of Pharm. in 1996, and the Ph.D. degree in 1999, from Kyushu University under the supervision of Prof. Koga. He was appointed as a research associate at the Faculty of Pharmaceutical Sciences of Kyushu University in 1999. His current researches have focused on molecular magnetism and creation of new optically functional materials by using transition metals and organic spin compounds.